Modelling the drying shrinkage of porous materials by considering both capillary and adsorption effects

Ginger El Tabbal, Patrick Dangla, Matthieu Vandamme, M. Bottoni, S. Granet

Version of Record: https://www.sciencedirect.com/science/article/pii/S0022509620302519
Manuscript_20fde3fdb63aa8ebd17eb471ee23ebc9

Modelling the Drying Shrinkage of Porous Materials by Considering both Capillary and Adsorption Effects

G. EL TABBAL[1, 2,3], P. DANGLA[2], M. VANDAMME[2], M. BOTTONI[1,3], S. GRANET[1,3]

1 : IMSIA, UMR9219, EDF-CNRS-CEA-ENSTA Paris Tech, France
2 : Université Paris-Est Laboratoire Navier (UMR 8205) CNRS, Ecole des Ponts Paris Tech, IFSTTAR, France
3 : EDF R&D, 7 bd Gaspard Monge, 92120 Palaiseau, France

Abstract

This paper presents a poromechanical model for drying of unsaturated porous media valid for a large range of relative humidity. Using the proper laws of thermodynamics, this model is derived and permits to account for different effects that contribute to the effective stress development: the average pore pressure effect, the energy of the interfaces effect, the surface adsorption effect and the Shuttleworth effect. The majority of the input parameters of this model are simply assessed by using two commonly known techniques for the characterization of pores structures applied on experimental desorption isotherms: the B.E.T theory (Brunauer et al., 1938) and the BJH technique (Barrett et al., 1951). Another input parameter (linked to the Shuttleworth effect) is fitted on experimental drying shrinkage strains. This model is tested and validated with experimental data for different porous materials - hardened ordinary cement paste, high- performance concrete and Vycor glass - found in the literature. The obtained results show a satisfactory evaluation of the drying shrinkage strains for all three tested materials, with the possibility of considering zero fitting parameter. Compared to other poromechanical models found in the literature such as the classical Biot-Bishop (Biot, 1941) model and the (Coussy et al., 2003) model, our model appears to be exclusively capable of displaying the transition at a certain relative humidity between the capillary pressure effects and the surface adsorption effect, which manifests itself by a plateau in the drying shrinkage strains curve at this value of relative humidity.

Key words: Porous material, Constitutive behaviour, Elastic material, Adsorption, Concrete

1 Introduction

The macroscopic constitutive behavior of a porous material subjected to a variation of the pore fluid pressure has been widely investigated. In the 1920s, Terzaghi introduced the notion of effective stress σ' in a porous body, i.e. the difference between the total stress σ applied on the considered body and the fluid pore pressure P_f. Posteriorly, the works of (Biot, 1941) and (Biot and Willis, 1957) initiated the poroelasticity approach for isotropic elastic saturated porous bodies. In the absence of external stresses, the latter approach made it possible to evaluate the corresponding volumetric strains ε by the mean of the pore pressure: $\varepsilon = (b/K_b) \cdot P^*$ where P^* is the pore pressure and is equal to P_f for a fluid-saturated porous body, b is the Biot coefficient written as $b = 1 - K_b/K_s$ for a porous body with a homogeneous solid skeleton, in which case K_b is the elastic bulk modulus of the material and K_s is the elastic bulk modulus of the solid skeleton. For a partially saturated porous body with two or more fluids occupying the pores, the works of Terzaghi and Biot were extended afterwards by (Bishop and Blight, 1963). In this approach, the pore pressure was written as a weighted average sum of the fluid pressures with a weighting coefficient χ. For instance, if we consider a porous body with a liquid phase (of a pressure P_L) and a gas phase (of a pressure P_G) occupying the pores volume, P^* will be written as:

$$P^* = \chi P_L + (1 - \chi) P_G \qquad (1)$$

χ is known as the Bishop parameter. This parameter depends essentially on the saturation of the porous body: $\chi = 1$ if the porous body is fully saturated and $\chi = 0$ if the body is completely dried. It was replaced in the works of (Lewis and Schrefler, 1987), (Hassanizadeh and Gray, 1980), (Hutter et al., 1999), by the water degree of saturation S_w. This postulation was expansively examined by (Gawin et al., 2006), (Gawin et al., 2006) and (Pereira et al., 2010).

By accepting this notion $\chi = S_w$ and defining a capillary pressure P_C as the difference between the gas pressure and the liquid pressure (i.e. $P_C = P_G - P_L$), the volumetric strains can be assessed from the following equation (in which the reference state from which strains are calculated is a state in which the pore space is saturated with a fluid at atmospheric pressure, and in which the pressure of the gas is assumed to remain equal to the atmospheric pressure):

$$\varepsilon = \left(\frac{b}{K_b}\right) P^* = -\left(\frac{b}{K_b}\right)(S_w P_C) \qquad (2)$$

This equation is known as the Biot-Bishop model. An extension of this model was established by (Coussy et al., 2003) who substituted the average pore pressure with an equivalent pore pressure π that also takes into account the contribution of the interfaces energy, noted as U. This term could be calculated from sorption/desorption tests by considering its dependency solely on the water saturation S_w: $U(S_w) = \int_{S_w}^{1} P_C(S_w) \cdot dS_w$. The evaluation of the volumetric strains by the (Coussy et al., 2003) approach is done with equation (3):

$$\varepsilon = (b/K_b)\pi = -\left(\frac{b}{K_b}\right)(S_w P_C + U) \qquad (3)$$

In the two previously introduced approaches (Biot-Bishop (Biot, 1941) and (Coussy et al., 2003)), the capillary pressure is considered to be the driving mechanism of the drying/wetting of the partially saturated porous materials. Similar approaches based on capillary mechanisms have been introduced by (Gawin et al., 2006), (Vlahinić et al., 2009), and (Rougelot et al., 2009). Nevertheless, the driving mechanisms of the drying/wetting of porous materials have been frequently debated in the literature. For instance, (Beltzung and Wittmann, 2005) considered that in hindered adsorption areas, the disjoining pressure (i.e. the difference between a mechanical pressure and thermodynamic pressure in the adsorbed layer of water) is hereby the principal mechanism of drying/wetting. Based on this approach, (Maruyama, 2010) elaborated an empirical relation that links the changes in the disjoining pressure in hardened cement pastes (calculated from drying shrinkage volume changes) to the experimental thickness of the adsorbed layer of water (assessed from sorption experiments while using a BET specific surface area). For mesoporous materials, (Ravikovitch and Neimark, 2006) first showed thermodynamically that adsorption induces a mechanical stress (sometimes called 'adsorption stress') whose magnitude is equal to the solvation pressure.

All the previously cited models were compared in the works of (Wyrzykowski et al., 2017) and it was shown that for a low relative humidity (lower than 40%-50%) those models fail to describe drying shrinkage experiments on an extended range of relative humidity. A possible explanation has been given by the authors that linked this failure to experimental uncertainties in the assessment of the experimental water degree of saturation. But this failure could also at least be partly due to the fact that those models neglect the energy contribution of the presence of adsorbed water (also called the surface energy effect (Setzer and Duckheim, 2009)). In fact, when the relative humidity decreases, a fraction of the pores are emptied from their bulk water but an adsorbed film of water (with a thickness that can reach several molecules) is deposed at their solid surface. This adsorption can modify the surface energy γ of the solid walls of the pore (according to Gibbs's isotherm (Gibbs, 1928)) and the surface stress σ_s to which those pore walls are submitted. Following (Kovler and Zhutovsky, 2006), this surface stress is mainly responsible for the shrinkage of the porous body when the relative humidity becomes smaller than 40%-50%, (i.e. when the fraction of unsaturated pores becomes important). This effect was regularly acknowledged in the literature (Wittmann, 2008), (Setzer et al., 2006), (Lura et al., 2003). In order to evaluate the drying/swelling strains induced by those surface effects, many refer to the works of (Bangham, 1931) that link the strains to the change of the surface energy γ. The empirical relation given in (Bangham et al., 1934) is written as: $\varepsilon = \lambda \cdot \Delta\gamma$ with λ a proportionality factor that depends on the material properties. This relation was at first elaborated by Bangham for charcoal materials but has later shown prominent results when used for modelling the drying shrinkage of other porous material such as Vycor glass (Hiller, 1964), (Bentz et al., 1998) and cementitious materials (Koenders and Van Breugel, 1997). This relation has been recently reviewed by (Gor and Bernstein, 2016a) who showed that, in the general case, Bangham's law is only an approximation. Like (Kramer and Weissmüller, 2007), they emphasize the fact that surface energy and surface stress are different thermodynamic entities and that, in systems in which surface effects prevail, strains are governed by variations of surface stress rather than of surface energy. However, (Gor and Bernstein 2016) showed that Bangham's equation should be verified for small strains and small adsorbed molecules with non-specific interactions, in which case the variations $\Delta\gamma$ of the surface energy are approximately equal to the variations $\Delta\sigma_s$ of the surface stress.

Despite the success of the Bangham's law in evaluating drying/swelling strains at low relative humidity range and in taking into account surface energy effects, this relation remains empirical. A thermodynamic extension of poromechanics to account for surface energy effects in absence of capillary effects can be found in (Vandamme et al., 2010) and (Zhang, 2018). In materials with a wide pore size distribution in contact with a gas at a generic partial pressure, some (smaller) pores are filled with fluid while some other (larger) pores are not filled but have their surface covered with adsorbed fluid. Consequently, in the generic case, a proper model for fluid-induced deformation of partially saturated porous solids should take into account both capillary effects and the effect of fluid adsorption at the surface of already unsaturated pores. The main aim of this work is to derive such a model. It is important to point out that comparable attempts were earlier made in the literature. For instance, while treating porous materials with a unique size of pores, (Balzer et al., 2017) and (Gor et al., 2018) calculated the fluid-induced strains by using surface-energy/stress-based models prior to the occurrence of the capillary condensation and by referring to capillary-based models after the capillary condensation takes place. On another hand, (Rahoui, 2018) accounted for both capillary and fluid adsorption effects with a phenomenological combination of the (Coussy et al., 2003) model and Bangham's law. Finally, (Rahimi-Aghdam et al., 2019) proposed a thermodynamic formulation based on a Gibbs energy potential that considers both capillary and fluid adsorption effects. The latter formulation was extended in (Nguyen et al., 2020) so it could be valid for confined nanopores with hindered adsorbed water layers.

The following section describes the porous system considered in this work along with the interfaces at play. The corresponding constitutive model is derived in section 3 and is then validated by experimental drying shrinkage strains results in section 4.

2 Description of the porous system and thermodynamic considerations

2.1 Distribution of water in pores

In order to develop a poromechanical model that takes into account both the capillary and the fluid adsorption effects, we begin by defining the considered porous system. The derived thermodynamic model in this work is valid for systems formed

by mesopores and macropores (i.e. systems with pores larger than two nanometers). The derivation is established under the frame of thermodynamics of continuum medium while considering isothermal transformations ($dT = 0$). The local state postulate allows us to address the thermodynamics of continuum medium while considering that the thermodynamic equations written for any system of volume V results from the combination of the thermodynamic equations written for infinitesimal elementary volumes extracted from the total system (Coussy, 2004). Therefore, the following thermodynamic derivation is considered to be written for a local elementary volume V_0. It is important to note that all the posteriorly derived equations are written with physical quantities expressed per unit volume V_0.

The studied elementary volume is assumed to be formed by a solid matrix and a connected porous network formed by saturated pores and unsaturated pores (Fig. *1*). This system is put into contact with a fluid at a given partial pressure. The reasoning can be applied to any fluid, but here we consider water. Some (smaller) pores may contain liquid water, while some (larger) pores may contain gas.

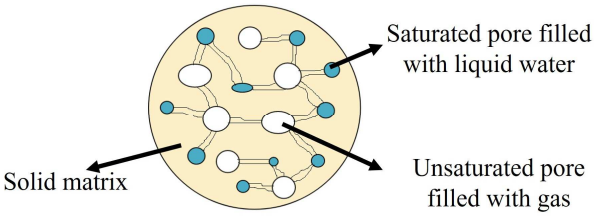

Fig. 1 - Schematics of the considered porous medium

We consider that the unsaturated pores have their bulk volume V_G filled with a gas phase composed of N_{vp} moles of water vapor and N_{dra} moles of dry air (as we will see later on, an additional amount of water is adsorbed on the unsaturated pores surface). As for the saturated pores, we consider that their bulk volume V_L is filled with a liquid phase composed of N_{lq} moles of liquid water.

It should be noted that between the previously considered phases α (gas or liquid phase) and β (the solid surface of the unsaturated or saturated pores), there exists a transition zone or interface region in which the composition is not homogeneous and does not correspond to those of α and β (Maugis, 1980). Several physical quantities (e.g. the volume concentration) vary according to the distance from this interface region (Fig. 2-a). Hence, to model this system, (Gibbs, 1928) proposed to define an ideal system with a dividing surface or interface **Σ** located in the transition zone and to assume that the composition of the neighboring phases remains homogeneous until reaching this surface (Fig. 2-b).

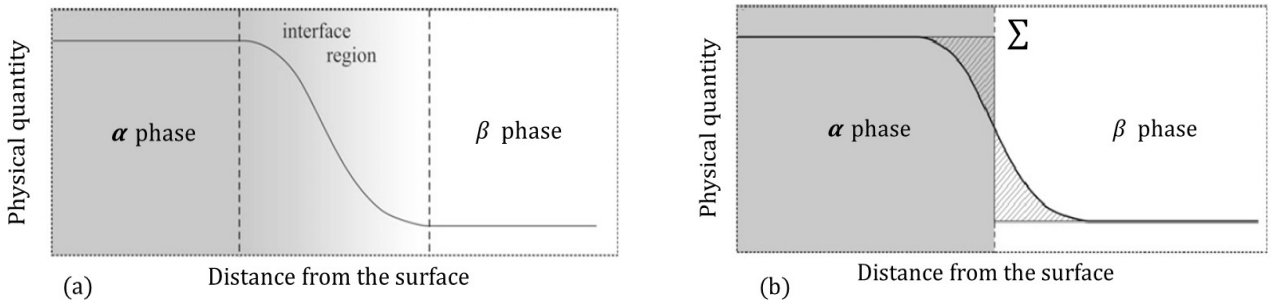

Fig. 2- (a) The system with the interface region (b) The Gibbs system for the interface, adapted from (Gyozo G. and Cesar A., 2012)

In the Gibbs system, the total number N of moles (per unit volume) of the considered component in the system is equal to:

$$N = N_\alpha + N_\beta + N_{ex} \tag{4}$$

where N_α and N_β are the number of moles (per unit volume) of the component found in the phases α and β , respectively; N_{ex} is the number of moles of the component (per unit volume) placed in excess on the interface so that the total number of moles in the initial system and the Gibbs system is the same.

By applying Gibbs' vision to the porous system considered in this work, the interfaces **Σ** that will be put at play are: interfaces between solid and gas phases in the unsaturated pores, interfaces between solid and liquid in the saturated pores and interfaces between liquid and gas phases (see Fig. *3*). Regarding the excess moles to be placed on those interfaces, two assumptions are made in the current framework. First, at the solid surface of the saturated pores, no transition zone is to be considered (no water excess moles will be placed at the solid/liquid interface), which could be justified by relatively equal densities of the adsorbed water and the liquid water found in those pores (Powers and Brownyard, 1947) and by an appropriate choice of the location of the Gibbs' interface. Second, at the solid/gas interfaces, the excess moles N_{ex} are considered to be

principally composed of water (see Fig. 3). It could be finally noted that in the unsaturated pores, the number of water moles is $N_{ex}+ N_{vp}$, whereas the total number of water moles in the previously defined system is $N_{ex}+ N_{vp} + N_{lq}$.

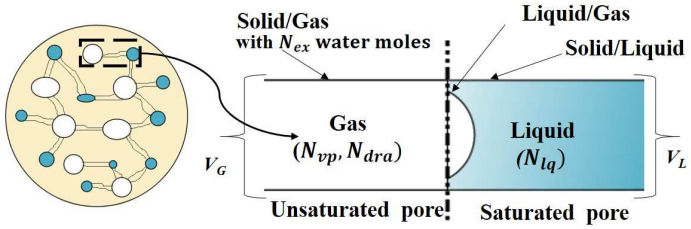

Fig. 3- Schematics of the considered porous medium

2.2 Surface energy and surface stress

The work of (Gibbs, 1928) makes it additionally possible to generalize equation (4) for any extensive physical quantity X and to define an excess physical quantity X_{ex} located on the interface. Subsequently, being an extensive quantity, an excess Helmholtz free energy F_{ex} (per unit volume) for the solid/gas interface can be defined. The latter free energy can be written as (Coussy, 2010):

$$F_{ex} = \gamma A_{S/G} + \mu N_{ex} \tag{5}$$

where γ is the surface energy of the solid/gas interface, $A_{S/G}$ its surface area per unit volume, N_{ex} the number of water excess moles per unit volume and μ the chemical potential of the corresponding excess moles of fluid.

The variation dF_{ex} of the free energy of the interface can be linked to the variation $dA_{S/G}$ of the interface surface area and to the variation dN_{ex} of the number of excess moles. According to thermodynamics (Maugis, 1980),(Weber et al., 1988),(Andrieu and Muller, 2005), the surface area of an interface can be increased either by adding new moles to its surface or by straining the surface at a constant number of moles. We define A_{cre} as the contribution (per unit volume) to the increment of the interface surface area linked to the process of creation of new moles and A_{def} as the contribution (per unit volume) corresponding to the deformation of the existing interface surface area. Accordingly dF_{ex} can be written as (Weber et al., 1988):

$$dF_{ex} = \sigma_s dA_{def} + \gamma dA_{cre} + \mu dN_{ex} \tag{6}$$

where σ_s is called the surface stress and γ is the surface energy (also known as the surface tension). It is important to distinguish between these two terms. This distinction has been previously discussed in the literature (Kramer and Weissmüller, 2007). (Vandamme et al., 2010),(Gor and Bernstein, 2016b),(Schulman et al., 2018): while γ is the energy needed to create a new surface of area A at a constant structure (by adding new moles to the surface or by cleavage), σ_s is the force that opposes an elastic strain of the surface, changing the intermolecular distance at a constant number of moles at the surface (Kramer and Weissmüller, 2007).

By combining equation (6) with the derivative of equation (5) we obtain the Gibbs-Duhem relation (Weber et al., 1988):

$$-(\sigma_s - \gamma)A_{S/G}\, d\varepsilon_s + A_{S/G} d\gamma + N_{ex} d\mu = 0 \tag{7}$$

where $d\varepsilon_s$ $(= dA_{def}/\, A_{S/G}\,)$ is defined as the interface surface strain. In equation *(7)*, we can identify two commonly used relations:

i. If the surface is undeformable ($dA_{def} = 0$), then equation *(7)* becomes simply:

$$A_{S/G} d\gamma = -N^{ex} d\mu \tag{8}$$

Equation (8) is known as the Gibbs adsorption isotherm relation (Gibbs, 1928). It links the decrease of the surface energy to the adsorption. In this equation, we can define a density of excess moles at the interface per unit surface noted as $\Gamma = N^{ex}/A_{S/G}$. If the number of excess molecules does not depend on the deformation of the surface, i.e. if Γ depends only on the chemical potential μ of the adsorbate, equation (8) can be integrated from an initial (dry) state where no excess moles are found on the interface:

$$\gamma = \gamma_1(\varepsilon_s) - \int_{-\infty}^{\mu} \Gamma(\mu) d\mu \;\; = \gamma_0(1 + \alpha\varepsilon_s) \; - \int_{-\infty}^{\mu} \Gamma(\mu) d\mu \tag{9}$$

$\gamma_1(\varepsilon_s)$ is the surface energy before adsorption that depends on the deformation state of the interface. In this work we consider that $\gamma_1(\varepsilon_s)$ is a linear function of ε_s with $\gamma_1(\varepsilon_s) = \gamma_0(1 + \alpha\varepsilon_s)$, γ_0 is the surface energy of the un-deformed surface and α is a constant coefficient if surface strains are sufficiently small.

ii. From equation *(7)*, we can identify the Shuttleworth relation (Shuttleworth, 1950):

$$\sigma_s = \gamma + \frac{\partial \gamma}{\partial \varepsilon_s}\bigg|_{\mu} \tag{10}$$

If we combine equation (9) and equation (10), we obtain the following equation (by considering only the zeroth-order terms and that Γ does not depend on the deformation of the surface, the latter being a reasonable assumption in the case of adsorption with non-specific interactions (Gor and Bernstein, 2016)):

$$\sigma_s = \gamma_0(1 + \alpha) - \int_{-\infty}^{\mu} \Gamma(\mu) d\mu \tag{11}$$

3 Constitutive model

3.1 Notions of Lagrangian porosity and Lagrangian saturation

When talking about a variable describing the system and evolving in time, it is important to indicate the reference state considered. In this frame, we write all equations within a Lagrangian approach. Accordingly, the Lagrangian porosity denoted by ϕ is equal to the ratio of the current volume of pores V_p with respect to the initial volume V_0 (Coussy, 2004). An increment φ in the Lagrangian porosity can therefore be defined as:

$$\varphi = \phi - \phi_0 \tag{12}$$

where ϕ_0 is the initial porosity of the system (i.e. the initial volume of pores $V_{p,0}$ divided by V_0). Moreover, we define ϕ_L as the Lagrangian partial porosity filled with a liquid phase and ϕ_G as the one filled with the gas phase and the adsorbed water film. Those partial porosities verify the relation: $\phi = \phi_L + \phi_G$.

The partial porosity ϕ_α can be written as in (Coussy, 2007) :

$$\phi_\alpha = S_\alpha \phi_0 + \varphi_\alpha \tag{13}$$

where φ_α is the change of the partial Lagrangian porosity of the phase α. The term φ_α represents the contribution of the deformation process in the partial porosity ϕ_α. The term $(S_\alpha \phi_0)$ represents the contribution of the porous invasion by a phase α in the partial porosity ϕ_α , or also the partial porosity before any deformation. S_α is the Lagrangian saturation, which can be defined as the ratio between the initial volume of pores that are currently filled by the phase α (i.e., the volume of those pores prior to any deformation noted as $V_{\alpha,0}$) divided by the initial volume of pores $V_{p,0}$. Under the frame of this work, S_L is the Lagrangian volume fraction of the saturated pores and S_G the Lagrangian volume fraction of the unsaturated pores.

This definition for Lagrangian saturation will allow us in the following section to separate the contributions to the energy balance related to the invasion process and to the deformation process (see Equation (25)).

3.2 Constitutive equations

With the purpose of deriving the constitutive laws of poromechanics for the considered system, the energy balance of the solid matrix must be correctly written. To this end, the following procedure is adopted:

i. We write the energy balance of the considered elementary volume V_0.
ii. We subtract the energy contribution of the different components considered in section 2.1 from the total energy balance of the system.
iii. We subtract the energy contribution due to the presence of adsorbed water at the solid/gas interface. The balance energy for the solid skeleton (solid matrix + solid/gas, solid/liquid and liquid/gas interfaces) is obtained.
iv. We subtract the energy contribution of the three interfaces: solid/gas – solid/liquid – liquid/gas. The energy balance of the solid matrix is obtained.

The transformations in this system are considered to be reversible: first, because they are so slow that viscous dissipations are negligible and then because the solid skeleton is considered to be elastic. Hence, let us remind that the variation of the Helmholtz free energy dF (per unit volume) for the system of interest, formed by multiple phases and undergoing reversible isothermal evolutions can be written as (Coussy, 2004):

$$\mathrm{d}F = \delta W + \sum_i \mu_i \, dN_i \tag{14}$$

where δW is the quantity of mechanical work exchanged with the external environment (per unit volume), μ_i is the chemical potential of the ith component and N_i its number of moles (per unit volume).

i. By referring to equation (14) the mechanical work provided to this volume is equal to the work of the external forces:$\delta W = \sigma d\varepsilon$, σ and ε are respectively the stress and strain developed in the volume V_0 of the porous system.

The number of moles components (per unit volume) present in the considered volume are as defined in section 2.1: N_{lq} moles of liquid water, N_{vp} moles of water vapor, N_{dra} moles of dry air and N_{ex} excess water moles placed at the solid/gas interface. It is important to note that at thermodynamical equilibrium of the system, the water under its different phases (vapor, liquid, adsorbed) is at a given chemical potential μ_w. Accordingly, equation (14) will be then written as:

$$dF = \sigma d\varepsilon + \mu_w dN_{lq} + \mu_w dN_{vp} + \mu_{dra}\, dN_{dra} + \mu_w dN_{ex} \tag{15}$$

ii. As a second step, we subtract from equation (15) the variation dF_i of the Helmholtz free energy (per unit volume) of each of the components. The latter can be written by analogy to equation (14) while considering that the corresponding mechanical work δW is purely hydrostatic and equal to $-P_i\, d\phi_i$, with P_i being the thermodynamical pressure and ϕ_i the Lagrangian volume fraction occupied by the i^{th} component. dF_i is then written as:

$$\mathrm{d}F_{lq} = -P_{lq}\, d\phi_L + \mu_w\, dN_{lq} \tag{16}$$

$$\mathrm{d}F_{vp} = -P_{vp}\, d\phi_G + \mu_w\, dN_{vp} \tag{17}$$

$$\mathrm{d}F_{dra} = -P_{dra}\, d\phi_G + \mu_a\, dN_{dra} \tag{18}$$

In the above equations, the water vapor and the dry air occupy the same volume fraction ϕ_G of unsaturated pores while the liquid water occupies the volume fraction ϕ_L of saturated pores. Equations (16) to (18) are subtracted from equation (15) while considering that the gas is ideal, so that the gas pressure P_G is equal to the sum of the vapor water pressure and the dry air pressure $P_G = P_{vp} + P_{dra}$:

$$dF - dF_{lq} - dF_{vp} - dF_{dra} = \sigma d\varepsilon + P_L d\phi_L + P_G d\phi_G + \mu_w dN_{ex} \tag{19}$$

iii. As a third step, we aim to subtract from the energy balance *(19)* the increment of the free energy (per unit volume) due only to the presence of adsorbed water at the solid/gas interface. This energy is noted as F_{ads} and can be expressed as:

$$F_{ads} = F_{ex} - F_{S/G} \tag{20}$$

F_{ads} is defined as the difference between the free energy F_{ex} of the solid/gas interface when the excess water molecules are adsorbed at its surface and the free energy $F_{S/G}$ of the same interface when no adsorption occurs.

In the purpose of correctly writing each of those energies, let us begin by defining the surface area of the considered solid/gas interface. As it has been indicated in section 2.2, the variation of this surface area $A_{S/G}$ could be linked to two processes:

- The straining of the considered interface at a constant number of moles. This contribution (per unit volume) is noted as A_{def}.
- The addition of new moles at the considered interface. This contribution (per unit volume) A_{cre} will be written for what follows as a product of $A_0\omega_G$ where A_0 is the total surface area of the pores (per unit volume) at the un-deformed state and ω_G a new variable that defines the Lagrangian surface fraction of the unsaturated pores in the porous body.

This previous consideration leads us to write $A_{S/G}$ as:

$$A_{S/G} = A_0\omega_G + A_{def} \tag{21}$$

It could be brought to attention that the previous expression of $A_{S/G}$ is similar the expression of ϕ_α given in equation (13). Once the different contributions to the increment of $A_{S/G}$ are identified, by referring to equation (5), we can write $F_{ex} = \gamma A_{S/G} + \mu_w N_{ex}$ and $F_{S/G} = \gamma_0 A_{S/G}$. In the expression of $F_{S/G}$, γ_0 is the surface energy density prior to deformation and without adsorbed molecules. According to equation (6), we write dF_{ex} as:

$$dF_{ex} = \gamma d(A_0\omega_G) + \sigma_s dA_{def} + \mu_w dN_{ex} \tag{22}$$

And by differentiating the expression of $F_{S/G}$, we obtain:

$$dF_{S/G} = \gamma_0 d(A_0\omega_G) + \gamma_0 dA_{def} \tag{23}$$

Once equation (20) is differentiated, dF_{ads} is then subtracted from equation (19). The obtained energy $F_{sk} = F - F_w - F_{ad} - F_{vp} - F_{dra} - F_{ads}$ is defined as the free energy per unit volume of the solid skeleton (i.e. the solid matrix + all three interfaces with constant surface energy densities and with no water excess moles on the solid/gas interface). dF_{sk} is then written as (after noting $\Delta\gamma = \gamma - \gamma_0$):

$$dF_{sk} = \sigma d\varepsilon + P_L d\phi_L + P_G d\phi_G - (\sigma_s - \gamma_0) dA_{def} - \Delta\gamma d(A_0\omega_G) \tag{24}$$

After substitution of each of the partial porosities ϕ_L and ϕ_G by their corresponding expression given in equation (13) and while noting that $S_L + S_G = 1$ and $P_c = P_G - P_L$, we derive:

$$dF_{sk} = \sigma d\varepsilon + P_L d\varphi_L + P_G d\varphi_G - \phi_0 P_c dS_L - (\sigma_s - \gamma_0) dA_{def} - A_0\Delta\gamma d\omega_G \tag{25}$$

In the energy balance given by (25), we can clearly observe that the definition of a Lagrangian porosity and saturation has allowed the separation of the terms related to the pores invasion process (the two terms $-\phi_0 P_c dS_L$ and $-A_0\Delta\gamma d\omega_G$) from the terms related to the deformation process ($\sigma d\varepsilon, P_L d\varphi_L, P_G d\varphi_G$ and $-(\sigma_s - \gamma_0) dA_{def}$)).

If we consider that $A_{def} = A_{def}(\varepsilon, \varphi_L, \varphi_G, S_L)$, we can write:

$$dF_{sk} = (\sigma - \sigma_a) d\varepsilon + (P_L - P_L^a) d\varphi_L + (P_G - P_G^a) d\varphi_G - \phi_0 P_c dS_L - A_0\Delta\gamma d\omega_G \tag{26}$$

where:

$$\sigma_a = (\sigma_s - \gamma_0) \left.\frac{\partial A_{def}}{\partial \varepsilon}\right|_{\varphi_L, \varphi_G, S_L} \tag{27}$$

$$P_L^a = (\sigma_s - \gamma_0) \left.\frac{\partial A_{def}}{\partial \varphi_L}\right|_{\varepsilon, \varphi_G, S_L} \tag{28}$$

$$P_G^a = (\sigma_s - \gamma_0) \left.\frac{\partial A_{def}}{\partial \varphi_G}\right|_{\varepsilon, \varphi_L, S_L} \tag{29}$$

In equation (26), the term $(\sigma_s - \gamma_0) \left.\frac{\partial A_{def}}{\partial S_L}\right|_{\varepsilon, \varphi_L, \varphi_G}$ was neglected because it is considered to be very small with respect to the term $(\phi_0 P_c)$. In fact, the variation of A_{def} with respect to the Lagrangian degree of saturation is negligible compared to the variation of A_{def} with $\varepsilon, \varphi_G, \varphi_L$ (i.e. A_{def} is a contribution to the increment of the interface surface area primarily linked to the deformation process)

iv. By considering that constant surface energies are accounted for in the energy of the solid skeleton F_{sk}, the approach used in (Dangla and Pereira, 2014) can be used and F_{sk} can be subdivided as:

$$F_{sk} = F_{sol}(\varepsilon, \varphi_L, \varphi_G, S_L) + F_{int}(\varphi_L, \varphi_G, S_L) \tag{30}$$

F_{sol} is the free energy (per unit volume) stored in the solid matrix and F_{int} the free energy (per unit volume) stored at the interfaces. In equation *(30)*, F_{int} is not a function of the porous material strains; in fact, it depends on them only indirectly through the pores volumes and the saturation. According to (Dangla and Pereira, 2014):

$$F_{int}(\varphi_L + \lambda\phi_0 S_L, \varphi_G + \lambda\phi_0 S_G, S_L) = \left(1 + \tfrac{2}{3}\lambda\right) F_{int} \qquad \forall \lambda \ll 1 \tag{31}$$

Equation (31) indicates that from the current state, at a constant degree of saturation, any isotropic homothetic variation of the pore dimension by a factor $(1+\lambda/3)$ will induce a volume variation of $(1+\lambda)$ and a surface variation of $(1+2\lambda/3)$ (with $\phi_0 S_\alpha$ the initial volume of the considered pore in the undeformed state). This statement is valid regardless of the pores shape (see Appendix 2). The differentiation of equation (31) with respect to λ leads to:

$$\phi_0 S_L \left.\frac{\partial F_{int}}{\partial \varphi_L}\right|_{\varphi_G, S_L} + \phi_0 S_G \left.\frac{\partial F_{int}}{\partial \varphi_G}\right|_{\varphi_l, S_L} = \frac{2}{3} F_{int} \tag{32}$$

We perform a first-order expansion of F_{int} with respect to φ_L and φ_G:

$$F_{int} = \tfrac{2}{3} U_L(S_L)\varphi_L + \tfrac{2}{3} U_G(S_L)\varphi_G + \phi_0 U(S_L) \tag{33}$$

with $U(S_L)$ being the energy of the interfaces before any deformation process, per unit volume of porous solid. $U_L(S_L)$ and $U_G(S_L)$ are interfaces energies respectively associated with liquid and gas phases. By combining equations (32) and (33), we identify U_L and U_G as two functions that verify the following relation: $U = S_L U_L + S_G U_G$.

By equating the expression given in (26) with the derivative of equation (30), and knowing that $\partial F_{sol}/\partial S_L$ is negligible compared to $\partial F_{int}/\partial S_L$ and that the terms $\frac{2}{3}\varphi_L dU_L(S_L)$ and $\frac{2}{3}\varphi_G dU_G(S_L)$ are considered to be very small (assumption of small deformations and porosities), we obtain:

$$\frac{\partial Fint}{\partial S_L} = \phi_0 \frac{dU(S_L)}{dS_L} = -\phi_0 P_c - A_0 \Delta\gamma \frac{d\omega_G}{dS_L} \quad (34)$$

After integration of the above equation from a reference saturated state (considered for a relative humidity of 100%), we write:

$$U(S_L) = -\int_{S_{100}}^{S_L} P_c(S_L)\, dS_L - A_0/\,\phi_0 \int_{\omega_{100}}^{\omega_G} \Delta\gamma\, d\omega_G \quad (35)$$

In the above equation, the volume fraction of saturated pores for a relative humidity of 100% is considered to be equal to S_{100} ($S_{100} \leq 1$) and the surface fraction of unsaturated pores is equal to ω_{100} ($\omega_{100} \geq 0$). In fact, based on experimental observations of sorption tests found in the literature (Baroghel-Bouny et al., 1999),(Chen, 2013),(Mjahad, 2012), when a porous material is exposed to an atmosphere with a relative humidity approaching 100%, the pores (especially the large ones) are not necessarily fully saturated. This point will be further discussed (see section 4.5.1).

As a final step, we write the free energy (per unit volume) of the solid matrix as:

$$(dF_{sol})_{S_L} = (\sigma - \sigma_a)d\varepsilon + \left(P_L - P_L^a - \frac{2}{3}U_L\right)d\varphi_L + \left(P_G - P_G^a - \frac{2}{3}U_G\right)d\varphi_G \quad (36)$$

where $(dF_{sol})_{S_L}$ means that the differentiation is performed at constant liquid saturation S_L.

In equation *(36)*, we define $\pi_L = \left(P_L - P_L^a - \frac{2}{3}U_L\right)$ and $\pi_G = \left(P_G - P_G^a - \frac{2}{3}U_G\right)$ as the equivalent pore pressures associated respectively to the liquid and gas phases. The above equation will be used in the following section to write the poromechanical constitutive laws.

It should be noted that the above derived approach considers the presence of a "spreading pressure" (Gor et al., 2018) on the solid surface of the unsaturated pores. This is by considering a possible variation of both the longitudinal and transversal dimensions (radius and length in the case of a cylindrical pore) of a considered pore shape. However, according to equation *(30)* and appendix 2, in this approach this variation can only be identical for the different present dimensions (i.e.in the case of a cylindrical pore, the radius and length vary by the same factor (1+λ/3) given that in this approach a unique thermodynamic variable φ links the different dimensions of the pore).

3.3 Constitutive laws of poromechanics and the equivalent pore pressure

Once the free energy of the solid matrix is written, we define its Legendre-Frenchel conjugate function $F_{sol}^* = F_{sol} - \pi_L\varphi_L - \pi_G\varphi_G$ and $dF_{sol}^* = (\sigma - \sigma_a)d\varepsilon - \varphi_L d\pi_L - \varphi_G d\pi_G$. Within the frame of linear elasticity, F_{sol}^* must be a quadratic function with respect to the variables ε, π_L and π_G. Therefore F_{sol}^* is written as (Coussy, 2004):

$$F_{sol}^* = \frac{1}{2}K_b\varepsilon^2 - b_L\varepsilon\,\pi_L - b_G\varepsilon\,\pi_G - \frac{1}{2}\frac{{\pi_L}^2}{N_{LL}} - \frac{1}{2}\frac{{\pi_G}^2}{N_{GG}} - \frac{\pi_G \cdot \pi_L}{N_{LG}} \quad (37)$$

After comparing the expression of dF_{sol}^* with the derivative of equation (37), we will be able to write the following constitutive equations:

$$\sigma - \sigma^a = K_b\varepsilon - b_L\pi_L - b_G\pi_G \quad (38)$$

$$\varphi_L = b_L\varepsilon + \frac{\pi_L}{N_{LL}} + \frac{\pi_G}{N_{LG}} \quad (39)$$

$$\varphi_G = b_G\varepsilon + \frac{\pi_L}{N_{LG}} + \frac{\pi_G}{N_{GG}} \quad (40)$$

where K_b is the elastic bulk modulus of the porous medium; N_{LL}, N_{LG} and N_{GG} are the Biot moduli; b_L and b_G are the Biot coefficients associated respectively to the liquid and gas phases. The Biot coefficient of the porous medium is defined as $b = b_L + b_G$. When assuming that the saturated and unsaturated pores in the considered porous system undergo an iso-deformation (this hypothesis states that porous volume filled by each of the two considered fluids (liquid and gas) deforms in the same way whenever they are subjected to volumetric stresses but to no pressure and temperature variations (Coussy, 2007)), we come to find that $b_L = S_L \cdot b$ and $b_G = S_G \cdot b$. Those two relations allow us to write equation (38) as:

$$\sigma - \sigma^a = K_b\varepsilon - b(S_L\pi_L + S_G\pi_G) = K_b\varepsilon - b\pi \quad (41)$$

In the above equation, the equivalent pore pressure is defined as $\pi = (S_L\pi_L + S_G\pi_G)$. After replacing π_L and π_G by their expressions given in section 3.2, we write:

$$\pi = S_L P_L + S_G P_G - \frac{2}{3}U - (\sigma_s - \gamma_0)(S_L \frac{\partial A_{def}}{\partial \varphi_L}\Big|_{\varepsilon,\varphi_G,S_L} + S_G \frac{\partial A_{def}}{\partial \varphi_G}\Big|_{\varepsilon,\varphi_L,S_L}) \quad (42)$$

We consider that $\frac{\partial A_{def}}{\partial \varepsilon}\Big|_{\varphi_L,\varphi_G,S_L}$ is small compared to $\frac{\partial A_{def}}{\partial \varphi_L}\Big|_{\varepsilon,\varphi_G,S_L}$ and $\frac{\partial A_{def}}{\partial \varphi_G}\Big|_{\varepsilon,\varphi_L,S_L}$.By taking into account this assumption and by analogy with the approach adopted in (Dangla and Pereira, 2014):

$$A_{def}(\varphi_L + \lambda\phi_0 S_L, \varphi_G + \lambda\phi_0 S_G, S_L) = \left(1 + \frac{2}{3}\lambda\right) A_0 \omega_G \quad \forall \lambda \ll 1 \quad (43)$$

The derivation of equation (43) with respect to λ gives:

$$\frac{2}{3} A_0 \omega_G = \phi_0 S_L \frac{\partial A_{def}}{\partial \varphi_L}\Big|_{\varphi_G,S_L} + \phi_0 S_G \frac{\partial A_{def}}{\partial \varphi_G}\Big|_{\varphi_L,S_L} \quad 44)$$

After substitution of equation 44) and (35) in the equivalent pore pressure expression given by equation (42), we derive:

$$\pi = S_L P_L + S_G P_G + \frac{2}{3}\int_{S_{100}}^{S_L} P_c(S_L)\, dS_L + \frac{2}{3}(A_0/\phi_0)(\int_{\omega_{100}}^{\omega_G} \Delta\gamma\, d\omega_G - (\sigma_s - \gamma_0)\omega_G) \quad (45)$$

The last term of equation (45) can be integrated by parts (with $\Delta\gamma = \gamma - \gamma_0$):

$$\pi = S_L P_L + S_G P_G + \frac{2}{3}\int_{S_{100}}^{S_L} P_c(S_L)\, dS_L + \frac{2}{3}(A_0/\phi_0)(\int_0^{\gamma} \omega_G(S_L) d\gamma\ - (\sigma_s - \gamma)\ \omega_G(S_L)) \quad (46)$$

We replace the Gibbs isotherm relation (equation (8)) and the Shuttleworth relation (equation (10)) in the above expression. By replacing S_G with $1 - S_L$, the equivalent pore pressure π can be written as:

$$\pi = P_G - S_L\, P_C + \frac{2}{3}\int_{S_{100}}^{S_L} P_c(S_L) dS_L + \frac{2}{3}(A_0/\phi_0)\ (\int_0^{\mu} \omega_G(S_L)\ \Gamma\, d\mu - \left(\frac{\partial\gamma}{\partial\varepsilon_s}\right)\Big|_{\mu}\ \omega_G(S_L)) \quad (47)$$

Finally, from what has been mentioned in this section, we outline that the constitutive behavior law is given by equation (*41*) with the expression of the equivalent pore pressure given in (47). It should be noted that the assumption made earlier in this section of a negligible dependence of A_{def} with respect to the skeleton strains at constant partial Lagrangian porosities and saturation results in a zero adsorption stress in equation (41): $\sigma_a = (\sigma_s - \gamma_0)\frac{\partial A_{def}}{\partial \varepsilon}\Big|_{\varphi_L,\varphi_G,S_L} = 0$.

3.4 Contributions to the equivalent pore pressure π

It is important to note that in expression (47), each term underlines a specific contribution to the development of the equivalent pore pressure:

- The term $\boldsymbol{P_G - S_L P_C}$ (written also as $\boldsymbol{S_L P_L + S_G P_G}$) is the contribution of the average pore pressure.
- The term $\frac{2}{3}\int_{S_{100}}^{S_L} \boldsymbol{P_c(S_L)\, dS_L}$ is the contribution of the interfaces energy. Capillary effects are a consequence of all three terms: $\boldsymbol{P_G - S_L P_C} + \frac{2}{3}\int_{S_{100}}^{S_L} \boldsymbol{P_c(S_L) dS_L}$.
- The term $\frac{2}{3}(\boldsymbol{A_0/\phi_0})(\int_0^{\mu} \boldsymbol{\omega_G(S_L)\ \Gamma\, d\mu})$ is the effect of fluid adsorption.
- The last term $\frac{2}{3}(\boldsymbol{A_0/\phi_0})(-\left(\frac{\partial\gamma}{\partial\varepsilon_s}\right)\Big|_{\mu}\ \boldsymbol{\omega_G(S_L)})$ is the Shuttleworth effect.

By referring to other poromechanical models found in literature, it could be pointed out that the model by (Coussy et al., 2003) accounts only for the contribution of the average pore pressure and the interfaces energy. In contrast, the Bangham's model stands on the unique contribution of the fluid adsorption effects. On another hand, for fully saturated porous materials, the model proposed in (Vandamme et al., 2010) allows to consider the contribution of both the average pore pressure and the fluid adsorption effects. Finally the phenomenological derivation made in (Rahoui, 2018) allows to consider all three contributions of the average pore pressure, the interfaces energy and the fluid adsorption effects. However, in the work of (Rahoui, 2018), the Shuttleworth effect was not taken into account due to the difficulty to intuit such an effect without a proper thermodynamic derivation.

4 Application to drying shrinkage: comparison with experiments

The previously derived poromechanical model is used in this section to predict the strains induced by the drying of a porous material. Those strains can be evaluated according to equation (41). Given that, in a drying shrinkage experiment, the

total stress σ is equal to zero and that the material is considered to be isotropic, the drying shrinkage strain ε_d is equal to (1/3) of the total volumetric strain ε and can be written as:

$$\varepsilon_d = \frac{1}{3}\varepsilon = \frac{1}{3}\frac{(b\,\pi)}{K_b} \tag{48}$$

Equation (48) can be generalized to calculate a variation $\Delta\varepsilon_d$ with respect to any reference state as $\Delta\varepsilon_d = \frac{1}{3}\Delta\varepsilon = \frac{1}{3}\frac{(b\Delta\pi)}{K_b}$, where $\Delta\pi$ is the variation of equivalent pore pressure with respect to this same reference state.

4.1 Evaluation of the model input parameters

The assessment of the equivalent pore pressure π requires the calculation of various input parameters. In this work, the input parameters are evaluated with respect to the relative humidity h_R. The approaches or techniques adopted for this calculation are indicated in the list below. It should be noted that, to use the BJH method (Barrett et al., 1951) to calculate ω_G and S_L, we assume the pores to be cylindrically shaped.

- $\boldsymbol{P_G}$: the pressure of the gas phase is assumed to be constant and equal to the atmospheric pressure
- $\boldsymbol{S_L(h_R)}$: the Lagrangian saturation or volume fraction of the saturated pores at a given relative humidity is calculated with the BJH (Barrett et al., 1951) method (detailed in section 4.5)
- $\boldsymbol{P_C(h_R)}$: the capillary pressure for a given relative humidity is calculated with the Kelvin equation: $P_C = P_G - P_L = -(\rho_w RT)/M_w\ ln\ (h_R)$, where ρ_w is the liquid water density, R is the constant of ideal gazes, T is the ambient temperature
- $\boldsymbol{A_0}$: the total surface of the pores or specific surface area of the material per unit volume (m^2/m^3). A_0 is the product of the specific surface area (m^2/g) determined with the B.E.T (Brunauer et al., 1938) method or the BJH technique, by the experimental dry density ρ_{dry} (g/m^3).
- $\boldsymbol{\omega_G(h_R)}$: the surface fraction of the unsaturated pores at a given relative humidity is the ratio between the surface of the unsaturated pores at a given relative humidity obtained with the BJH method (see section 4.5) with respect to the total surface of pores (i.e. the specific surface area) calculated in section 4.3.
- $\boldsymbol{\phi_0}$: the initial porosity assessed by the processing of experimental data
- $\boldsymbol{d\mu}$: the total differential of the chemical potential of the adsorbed water in the unsaturated pores, calculated with the following equation derived from Kelvin equation: $d\mu = RTd\ln(h_R)$
- $\boldsymbol{\Gamma(h_R)}$: the number of the water excess moles per unit surface at the solid/gas interface equal to $\frac{\rho_w}{M_w}t(h_R)$ where $t(h_R)$ is the thickness of the multimolecular adsorbed layer of water at the surface of the unsaturated pores. In the case of water adsorption at a solid surface, $t(h_R)$can be evaluated by empirical relations such as (Badmann et al., 1981), (Hagymassy et al., 1969). In this work, $t(h_R)$ is evaluated using the (Badmann et al., 1981) relation (see section 4.4). We assume that the density of adsorbed water is that of bulk liquid water (Powers and Brownyard, 1947)
- $\left(\frac{\partial\gamma}{\partial\varepsilon_s}\right)\Big|_{\boldsymbol{\mu}}$: the Shuttleworth term. The value of this term depends highly on the morphology and the orientation of the solid surface (Weber et al., 1988). Although the (Shuttleworth, 1950) equation has been widely used (a review of this relation is given by (Cammarata, 1994)), how the surface energy γ varies with the skeleton strains is not obvious (Schulman et al., 2018). In this work, we propose to fit this term on experimental drying shrinkage strains.
- $\boldsymbol{K_b}$: the elastic bulk modulus K_b of the porous medium is considered to be constant (i.e., not to depend on the skeleton strains or on chemical potential μ). It is assessed by the processing of experimental data (see section 4.6.1).

4.2 Experimental results used for model validation

The predicted drying shrinkage strains are compared with experimental results given in the literature for three different porous materials:

- A hardened Portland cement paste with a water-to-cement ratio equal to 0.55, tested in (Maruyama et al., 2018). The corresponding experimental data are presented in section 4.2.1.
- A high-performance concrete with a water-to-cement ratio equal to 0.26, tested in (Baroghel-Bouny et al., 1999). The corresponding experimental data are presented in section 4.2.2.
- A Vycor glass (Corning 7930), tested by (Amberg and McIntosh, 1952) and reported by (Vlahinić et al., 2009). The corresponding experimental data are presented in section 4.2.3.

The above experimental data were chosen owing to the fact that the measured experimental points extend over a wide range of relative humidity, since we aim at examining the ability of the elaborated poromechanical model to capture both

capillary effects (which are expected to be dominant in the high relative humidity range) and fluid adsorption effects (which are expected to be dominant in the low relative humidity range).

For each of the considered experimental data, the experimental parameters and curves necessary for the model computation are:

- The experimental porosity ϕ_0[1] of the studied porous material.
- The dry density of the porous material ρ_{dry}[3] necessary for the computation of A_0.
- The water desorption isotherm that represents the hygral equilibrium states of the porous material when exposed to a decreasing relative humidity. This experimental curve could be represented either in terms of the experimental water degree of saturation[2] $S_w(h_R)$ or in terms of the experimental water content[3] $w(h_R)$. The dry reference state considered in the calculation of S_w or w has been found to differ from one experimental work to another. This point will be further discussed in the following sections.

  It should be noted that for the experimental data of (Maruyama et al., 2018) and (Amberg and McIntosh, 1952), the used desorption isotherms correspond to a subsequent (second) drying branch which could eventually avoid any irreversibility of the drying shrinkage following the use of the first drying branch. Regarding the high performance concrete studied by (Baroghel-Bouny et al., 1999), even though the desorption isotherm corresponds to a first drying branch, it could be considered (as stated in (Di Bella et al., 2017) and proven by (Maruyama, 2010)) that any possible observed irreversibility could be due to the presence of the well-known hysteresis in the sorption isotherm of cementitious materials and not due to the occurrence of a non-elastic phenomenon. Therefore, modelling drying shrinkage during a first drying by an elastic approach is considered to be acceptable (Di Bella et al., 2017).
- The elastic bulk modulus K_b of the porous medium.

4.2.1 Experimental results of (Maruyama et al., 2018)

The hardened cement paste (noted as hcp) studied in this work is prepared with a Japanese white Portland cement with a water-to-cement mass ratio equal to 0.55. After mixing, the cement paste was poured into 3x13x300 mm^3 molds. Following 180 days of curing under lime-saturated water, the hcp samples were placed into a chamber with a relative humidity of 11% chamber and equilibrated for more than 6 years. Sorption isotherms were obtained with a volumetric sorption analyzer (using an hcp powder) at different temperatures and consisted of a humidification process followed by a drying process. In this work we refer to the desorption isotherm (in terms of water content) obtained at 20°C with a relative humidity ranging from 0.97 down to 0 (Fig. 4-a). As for the dry reference state, the hcp samples were placed under vacuum at a temperature of 105°C at the end of the measurement. The experimental water content is normalized with respect to this mass. The water content when the relative humidity approaches zero, as seen in (Fig. 4-a), is not null, due to the fact that the drying of the sample at 105°C carries away more water than exposing the sample to a zero relative humidity at 20°C.

The measurement of the drying shrinkage strains was done with a LVDT (Linear variable differential transformer) for 3x13x300 mm^3 samples that were incrementally dried from $h_R = 0.9$ to $h_R = 0.11$. The values of the drying shrinkage strains vs h_R are given in (Fig. 4-b). The length of the sample at h_R =0.9 is considered to be the reference state. As for the porosity and the dry density of the considered hcp, no values for those parameters were given in the cited work. We referred to a porosity of a similar hardened cement paste (with a water-to-cement mass ratio of 0.5) studied by (Di Bella et al., 2017) where the dry reference state was equally taken by the authors for an oven drying at 105°C: in that case, the experimental porosity was $\phi_0 = 21\%$. As for the dry density of the hcp, an estimated value was later calculated and found to be compatible with the BJH calculation (details are shown in section 4.5).

---

[1] The experimental porosity is defined as $\phi_0 = \frac{m_{sat} - m_{dry}}{\rho_w V_0}$ with m_{sat} is the mass of the saturated sample and m_{dry} the mass of the dry sample, and ρ_w the density of water. The dry density of the sample is defined as $\rho_{dry} = \frac{m_{dry}}{V_0}$.

[2] The experimental degree of saturation is the volume fraction of the total water in pores (both the adsorbed water in unsaturated pores and the liquid water in saturated pores). It can be computed according to the relation: $S_w(RH) = \frac{m(RH) - m_{dry}}{m_{sat} - m_{dry}}$ with $m(RH)$ the mass at equilibrium of the sample exposed to a certain h_R.

[3] The experimental water content also relates to the total water in the pores and could be computed according to the relation: $w(RH) = \frac{m(RH) - m_{dry}}{m_{dry}}$. Having the previous relations in mind, one could relate S_w and w by: $S_w = \frac{w\,\rho_{dry}}{\phi_0\,\rho_w}$.

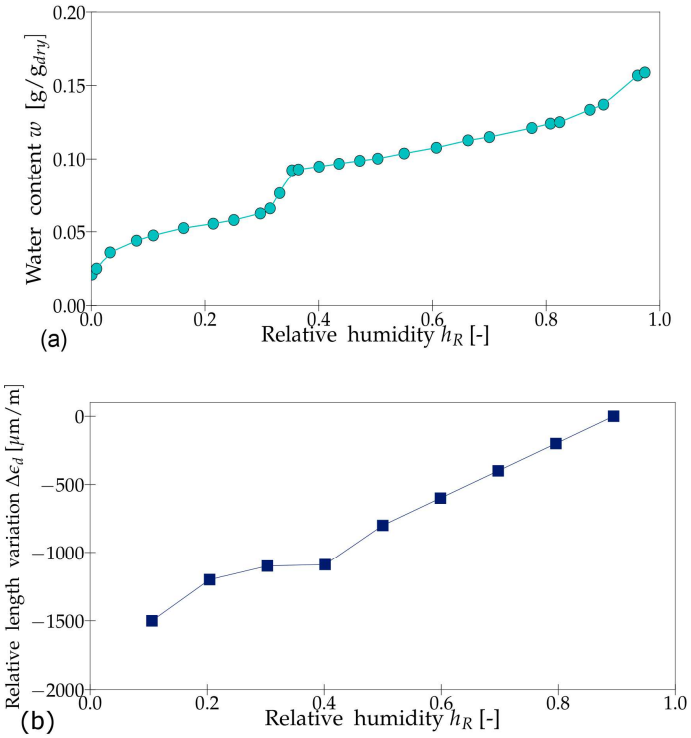

Fig. 4 – (Maruyama et al., 2018): (a) experimental water desorption isotherm – (b) experimental relative length variation

4.2.2 Experimental results of (Baroghel-Bouny et al., 1999)

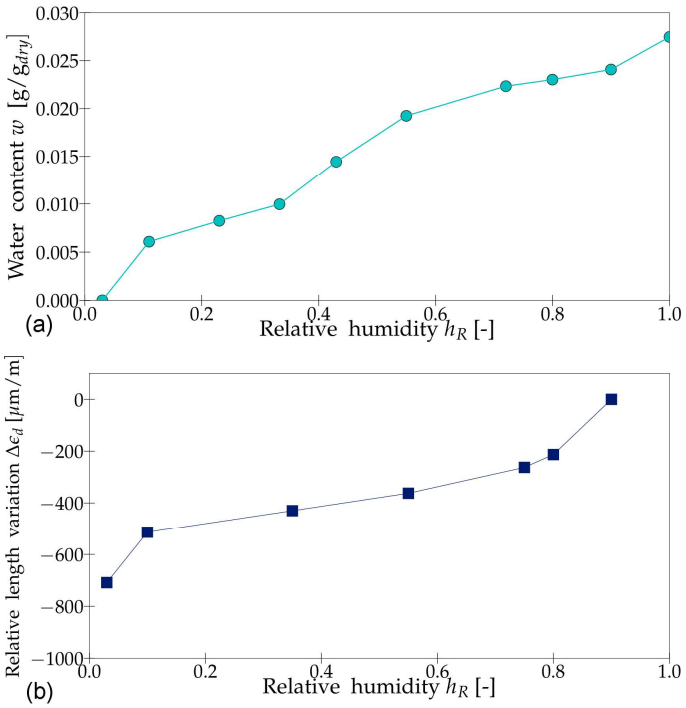

Fig. 5 – (Baroghel-Bouny et al., 1999): (a) experimental water desorption isotherm – (b) experimental relative length variation

The high-performance concrete tested by (Baroghel-Bouny et al., 1999) was prepared with a normal Portland cement with a certain fraction of silica fume and of superplasticizers. The specimens were discs with a 3 mm thickness and a 90 mm diameter. At the beginning of the tests, the concrete had an age of 1 year. The sorption test consisted of a drying process followed by a re-humidification process at a temperature of T=23°C. In this work, we refer to the desorption isotherm. The relative humidity varied between 1 and 0.03. The dry reference state was chosen to be the mass of the sample at h_R=0.03 and at an ambient temperature of T=23°C. By doing so, the authors wanted to avoid submitting the concrete to a drying process with conditions that differed from those of the desorption process; in fact, the risk with oven drying is that it could damage the specimen and so increase its porosity. Fig. 5-a displays the variation of the experimental water content with respect to h_R. This desorption isotherm can also be found in terms of the experimental degree of saturation in the work of (Baroghel-Bouny et al., 1999).

The samples used for the measurement of the drying shrinkage strains were identical to the ones used for the sorption test. The diameter and length of the discs were measured with dial gauges. By considering the diameter and length at h_R= 0.904 as an initial reference state, the values of the drying shrinkage strains vs. h_R are given in (Fig. 5-b). The porosity of the high-performance concrete is provided and is equal to 8.2%. The dry density, given also in the referred article, is equal to 2382 kg/m^3.

4.2.3 Experimental results of (Amberg and McIntosh, 1952)

The Vycor glass cited in the work of (Vlahinić et al., 2009) is a Vycor 7930 Corning glass that was originally tested by (Amberg and McIntosh, 1952). The desorption tests were done at a temperature of 11°C on rods of 11 cm length and 0.73 cm in diameter. The dry reference state is defined by (Vlahinić et al., 2009) as the mass of the sample at h_R=0.05.The desorption isotherm is given in terms of the degree of saturation (Fig. 6-a). The drying shrinkage strains are given in (Fig. 6-b) with an initial measurement reference taken for h_R=0.99. The porosity of this material is given by the manufacturer and is equal to 28% (Vlahinić et al., 2009). The dry density is equal to 1450 kg/m^3.

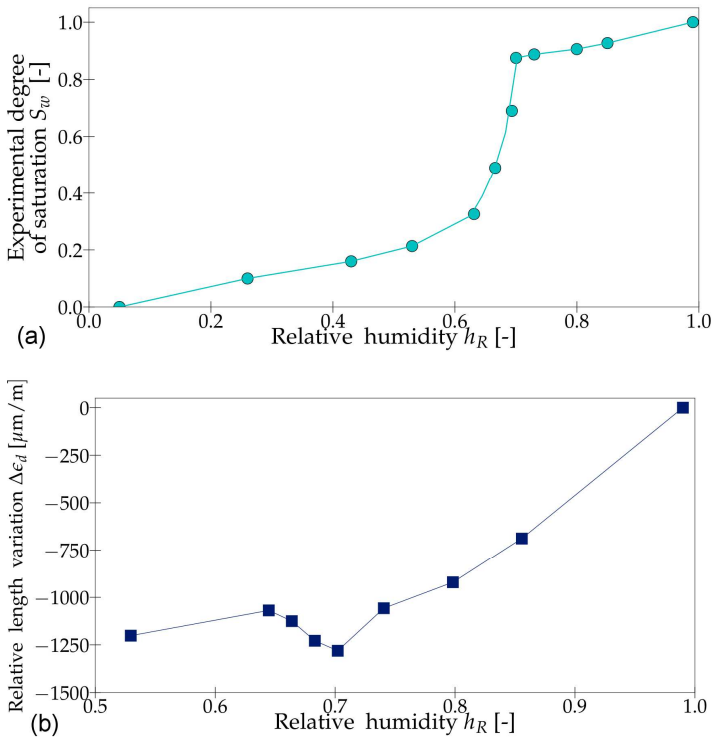

Fig. 6 – (Amberg and McIntosh, 1952): (a) experimental water desorption isotherm – (b) experimental relative length variation

4.3 Calculation of the specific surface area of the porous materials

There exist various methods for computing the specific surface area of a porous material. One of them is the gas sorption analysis technique, which uses water vapor or nitrogen adsorption tests. A comparison of this technique with other methods is given in (Thomas et al., 1999). In the present paper, we calculate the specific surface area of the materials using water vapor sorption isotherms with the BET (Brunauer et al., 1938) method. Due to its simplicity and ability to accommodate different

isotherms types, this method continues to be the most commonly used one for gas sorption specific surface area analysis (Aligizaki, 2006). The BET theory describes multimolecular adsorption on solid surfaces. This theory assumes that there is no adsorbate-adsorbate interaction. It also assumes that the adsorption of the first layer (i=0) is done with an energy of interaction E_0, while adsorption for all remaining layers (i>1) is done with an energy equal to the energy of liquefaction E_L (energy of a bulk liquid). When approaching saturation, the theory considers that the number of adsorbate layers becomes infinite. The BET theory is based on the following relationship (Aligizaki, 2006):

$$\frac{h_R}{(1-h_R)w} = \frac{1+(C-1)h_R}{C\,w_m} \tag{49}$$

where C is the BET constant linked exponentially to the molar heat of adsorption of the surface adsorbed molecules and thus to the hydrophilicity of the solid surface, w_m is the water content of the material when one layer of water covers the whole surface of the pores. Equation (49) allows for processing sorption experimental data so that the quantity $\frac{h_R}{(1-h_R)\cdot w}$ is plotted with respect to h_R. If the BET theory applies, a linear relationship must be obtained with a slope of $\frac{(C-1)}{C\,w_m}$ and a Y-intercept of $\frac{1}{Cw_m}$, so that it is possible to calculate w_m. In most cases, the BET theory applies in the region of h_R between 0.05 and 0.35 (Aligizaki, 2006). Indeed, in this region the hypotheses on which the theory relies are most likely verified. It is important to note that the classical BET theory is only valid for free adsorbed water layers rather that hindered ones. A modification of the classical BET theory in the case of hindered water spaces is proposed in (Nguyen et al., 2019). In the current framework, we consider that the pore spaces can only be filled with free adsorbed layers of water. Thus the classical BET theory remains valid.

Once w_m is calculated, we can then proceed to the evaluation of the specific surface area S_{BET} using the following equation (Baroghel-Bouny, 1994):

$$S_{BET} = \frac{N_A\,A_m\,V_m}{V_M} \tag{50}$$

where N_A is the number of Avogadro (6.023 10^{23} molecules/mol), A_m is the average area occupied by one molecule of the adsorbate: for water molecules, the value of 10.6 Å^2 is used in the literature (Baroghel-Bouny, 1994),(Hagymassy et al., 1969). V_M is the molar volume of water (18.10^{-6} m^3/mol (NIST Chemistry WebBook, 2018)) and V_m the volume of water (in m^3/g) corresponding to the value of w_m. The value of the specific surface area for each of the studied materials with the range of h_R where the BET theory is applied is given in Table 1.

Experimental Data	***Range of h_R where the BET theory is applied***	***Specific surface area S_{BET}***
(Maruyama et al., 2018)	0.11 – 0.30	157 m^2/g
(Baroghel-Bouny et al., 1999)	0.11 – 0.33	27 m^2/g
(Amberg and McIntosh, 1952)	0.25 – 0.43	81 m^2/g

Table 1- Specific surface area of the materials calculated with the BET theory

It is important to note that the value of the specific surface area calculated with the BET method depends highly on the number of experimental points used for the calculation. As far as the considered experimental data are concerned, the orders of magnitude obtained for the hardened cement paste and the high-performance concrete are in agreement with the literature: for a hardened cement paste, values of specific surface area are found to vary between 100 and 200 m^2/g (Baroghel-Bouny, 2007), while for high-performance concretes values are found to be around 20 m^2/g (Chen, 2013) (Baroghel-Bouny, 1994). As for the Vycor glass, the value calculated in Table 1 is lower than the values found in the literature. A value of 106 m^2/g obtained from water vapor isotherms is noted in (Gor and Bernstein, 2016b) and values ranging from 100 m^2/g to 173 m^2/g are given in (Bentz et al., 1998). The latter values were assessed from experimental nitrogen isotherms (with nitrogen isotherms known to provide smaller BET specific surface areas than the ones assessed from water vapor isotherms (Baroghel-Bouny, 1994)). The small specific surface area obtained in this work for the Vycor glass may be due to the limited number of experimental points that served in its computation. Indeed, only two experimental points were used in the BET calculation: the first one at h_R = 0.25 and the second one at h_R = 0.43. Therefore, for the experimental data of (Amberg and McIntosh, 1952), an alternative method for calculating the specific surface area is posteriorly proposed (see section 4.5.2).

4.4 Calculation of the thickness of the adsorbed layer of water

Concerning the thickness t of the adsorbed layer of water, the empirical relation given by (Badmann et al., 1981) is used in this work: $t(h_R) = K_1 + K_2\ln(-\ln(h_R))$. For each of the studied cementitious materials, we try to fit the values of K_1 and K_2 on the thickness t_{exp} of the adsorbed layer measured experimentally: $t_{exp} = V_{ads}/S_{BET}$ with V_{ads} the volume of adsorbed water assessed from the experimental water desorption isotherms. The obtained values are then compared to those given by (Badmann et al., 1981) for non-porous cement raw materials : $K_1 = 0.385$ nm and $K_2 = -0.189$ nm. The comparison is shown in Fig. 7.

We come to find that the values fitted on each of the experimental results ($K_1 = 0.42$ nm and $K_2 = -0.15$ nm for the experimental data of (Maruyama et al., 2018); $K_1 = 0.40$ nm and $K_2 = -0.21$ nm for the experimental data of (Baroghel-Bouny et al., 1999)) are in the vicinity of the values given by (Badmann et al., 1981). This small difference could be due to the different dry reference state taken by each of the authors while calculating the experimental water content. Nevertheless, we can admit that the (Badmann et al., 1981) values are mostly respected: we use those values in what follows.

As for the experimental data of the Vycor glass, no values for K_1 and K_2 were found in the works of (Badmann et al., 1981) for a similar composition. Therefore, K_1 and K_2 are fitted on the corresponding water isotherm. The values retained are: $K_1 = 0.33$ nm and $K_2 = -0.31$ nm.

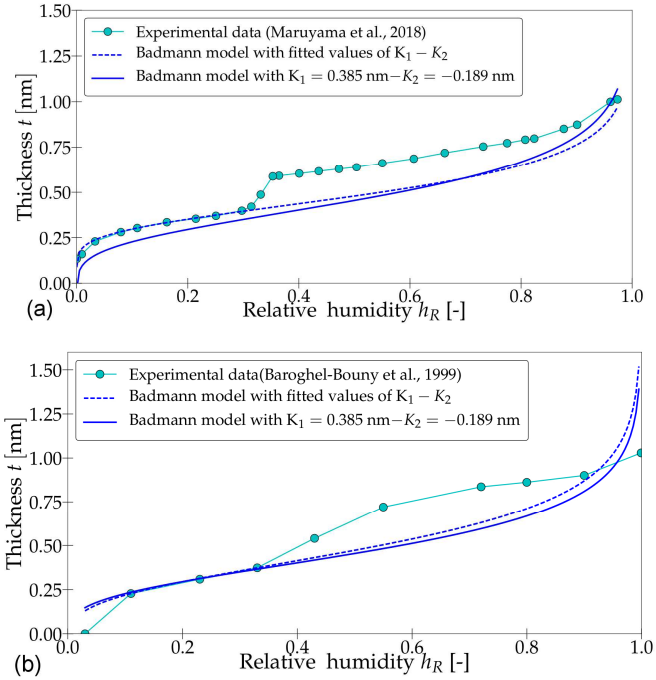

Fig. 7 – Experimental thickness of the adsorbed layer of water compared to the thickness given by the Badmann model: (a) experimental results of (Maruyama et al., 2018) with fitted values K_1= 0.42 nm and K_2=-0.15 nm – (b) experimental results of (Baroghel-Bouny et al, 1999)) with fitted values K_1= 0.40 nm and K_2=-0.21 nm

4.5 BJH method

The BJH method proposed by (Barrett et al., 1951) is used for the determination of the pore size distribution for porous media. In this method, the authors used the desorption branch. The pores were assumed to be cylindrically shaped and their radius noted r_p is equal to the sum of the Kelvin-Laplace radius[4] noted r_k and the thickness of the adsorbed layer t. The authors also assumed that the thickness of the adsorbed layer inside the pores is equal to that of an adsorbed layer on a flat surface.

4.5.1 Description of the method

The calculation process used in this method is detailed in (Rouquerol, 2003):

- By taking the water volume $V_{w,n}$ for each relative humidity h_R as an initial input (calculated from the experimental water desorption isotherm $w(h_R)$)[5], this method calculates the volume of desorbed water between two consecutive steps n-1 and n. This volume is noted as $\delta V_{w,n} = V_{w,n-1} - V_{w,n}$. It is important to note that seeking to avoid further integration complications, we tried fitting the experimental desorption isotherms with several models found in the literature (Van-Genuchten, 1980), (Durner, 1994), (Morandeau et al., 2014). However, the tested models were found incapable of precisely fitting the data in the range of relative humidity between 0.3 and 0.6. This range is important to model to observe the transition between the contribution of the capillary pressure and the fluid adsorption effects in the drying shrinkage process. Therefore, we proposed to linearly interpolate the experimental desorption isotherms before using them in the BJH calculation.

[4] The Kelvin-Laplace relation is written as $r_k = \frac{2\cdot\gamma}{P_G - P_L}$ where γ is the liquid-gas surface energy. The surface energy γ at a temperature T can be computed using the relation given in (IAPWS, 1992): $\gamma(mN/m) = 235.8 \cdot \left(1 - \frac{T}{T_c}\right)^{1.256} [1 - 0.625\left(\frac{T}{T_c}\right)]$ where T and T_c are expressed in Kelvin. T_c being the critical temperature of water ($T_c = 647.096\ K$)

[5] The volume of water in the pores can be calculated (per unit of dry mass) from the water content by $V_w = w/\rho_w$.

- Using the corresponding pore size $r_{p,n}(h_R) = r_{k,n}(h_R) + t_n(h_R)$, the method calculates a volume (noted $\delta V_{p,n}$) and an area (noted $\delta a_{p,n}$) that correspond to the class of pores that will be desaturated at a given h_R. The expression of $\delta V_{p,n}$ is given by equation *(51)* where $\overline{r_{p,n}}$ is the average radius of pores between two consecutive steps, $\delta t_n = t_{n-1} - t_n$ is the increment of the adsorbed layer thickness and $\delta a_{p,i} = 2\delta V_{p,i}/\overline{r_{p,i}}$ is the solid surface area under the assumption of cylindrical pores.

$$\delta V_{p,n} = \left(\frac{\overline{r_{p,n}}}{\overline{r_{p,n}} - t_n}\right)^2 [\, \delta V_{w,n} - \delta t_n \sum_{i=1}^{n-1} \delta a_{p,i}(1 - \frac{t_n}{\overline{r_{p,i}}})] \qquad (51)$$

- The cumulative sum of those volumes ($\sum_i \delta V_{p,i}$) corresponds to the total volume of the unsaturated pores at a certain relative humidity h_R. Knowing the total volume of pores per unit dry mass ($\phi_0 V_{m0}$) in the material (with V_{m0} the total volume of the sample per unit of dry mass), we can now compute the volume fraction of the unsaturated pores at a certain relative humidity h_R (previously noted as $S_G = \sum_i \delta V_{p,i} \,/(\phi_0\, V_{m0})$) and the volume fraction of the saturated pores at the same relative humidite ($S_L = 1 - S_G$). While the experimental degree of saturation S_w indicates the total fraction of water (adsorbed water + free liquid water) found in pores at a certain relative humidity, S_L designates exclusively the fraction of the free liquid water found in the pores at this relative humidity.

- The cumulative sum of areas (noted $\sum_i \delta a_{p,i}$) corresponds to the total area of the unsaturated pores at a certain relative humidity. Knowing the total surface of pores (which is, close to a multiplying factor, equal to the specific surface area of the material), we can calculate the surface fraction of the unsaturated pores for a given relative humidity (previously noted as ω_G and equal to the ratio of $\sum_i \delta a_{p,i}$ with respect to the specific surface area). The total area $\sum_i \delta a_{p,i}$ calculated at the final stage of the computation corresponds to a specific surface area of the material calculated with the BJH method S_{BJH}. It can be compared to the specific surface area S_{BET} assessed with the BET method (Table 1).

Before proceeding in the BJH computation, an important point on which relies this approach must be further discussed. This point consists on identifying the initial saturation state of the pores. In fact, for calculation purposes, this method assumes that in the initial reference state, the pores are completely saturated. Therefore, according to this technique, if the initial state is for a relative humidity approaching 1, the experimentally measured degree of saturation at this state $S_w(h_R \to 1)$ must be equal to 1. However, as it can be seen in the literature, this constraint is not always experimentally verified. For cementitious materials, (Baroghel-Bouny et al., 1999) noted $S_w(h_R \to 1)$=0.8 for the high-performance concrete studied in this work and $S_w(h_R \to 1)$=0.85 for other studied hardened cement pastes. Additionally, for high-performance concretes, (Chen, 2013) and (Mjahad, 2012) measured $S_w(h_R \to 1)$ of 0.8 and 0.9 respectively. Those experimental observations rely on the fact that submitting a porous material to a relative humidity approaching 1 may not induce a full saturation of the pores, which might only be reached by immersing the sample in liquid water.

Consequently, to be consistent with those experimental observations, for each of the cementitious materials studied in this work, the BJH calculation will start from a virtual state where the sample is considered to be fully saturated and then followed by the initial experimentally measured state (where the sample is exposed to a relative humidity approaching 1). For the latter state, we can consider that no water is adsorbed on the unsaturated pore surface (i.e. $S_L(h_R \to 1) = S_w(h_R \to 1)$). An example of the first steps of the BJH computation for the experimental data of (Baroghel-Bouny et al., 1999) is given in Table 2. The corresponding BJH results in terms of S_L and ω_G are shown in the following section.

Relative humidity	Water content	Water degree of saturati-on	Volume of water (cm^3/g)	Desorbed water volume (cm^3/g)	Volume of unsaturated pores (cm^3/g)	Area of unsaturated pores (m^2/g)	Total volume of unsaturated pores (cm^3/g)	Total area of unsaturated pores (m2/g)	Lagrangi-an gas saturation	Lagran-gian liquid saturation	Lagrang-ian surface fraction
h_R	w	S_w	$V_{w,n}$	$\delta V_{w,n}$	$\delta V_{p,n}$	$\delta a_{p,n}$	$\sum_i \delta V_{p,i}$	$\sum_i \delta a_{p,i}$	S_G	S_L	ω_G
Under water	-	1.0	$\phi_0 \cdot V_{0m}$ =0.0343	0.00	0.00	0.00	0.00	0.00	0.00	1.0	0.00
$h_R \to 1$	0.0274	0.8	0.0274	0.00690	0.00690	0.00128	0.00690	0.00128	0.20	0.80	$4.7\ 10^{-05}$
0.99	0.0271	0.79	0.0271	0.00033	0.00033	0.00012	0.0072	0.00140	0.21	0.79	$5.2\ 10^{-05}$
0.98	0.0268	0.78	0.0268	0.00033	0.00034	0.00832	0.0075	0.00973	0.22	0.78	0.0004
0.97	0.0265	0.77	0.0265	0.00033	0.00034	0.01511	0.0079	0.02485	0.23	0.77	0.0009

Table 2 – BJH computation of the experimental data of (Baroghel-Bouny et al., 1999)

Concerning the experimental data of (Maruyama et al., 2018), to calculate the fraction of the unsaturated/saturated pores, the total volume of pores per unit dry mass ($\phi_0\, V_{m0}$) must be known. However, as indicated previously (section 4.2.1), considering that the experimental porosity of the studied hcp was not cited in the mentioned article, we chose a value of ϕ_0=21% (Di Bella et al., 2017). On the other hand, given that sorption tests were done using powder samples, the volume V_{m0} was not measured in this work. Therefore, according to what was mentioned earlier in this section, we can assume that in the initial

experimentally measured state ($h_R = 0.97$) the experimental degree of saturation can take a value between 0.85 (value given in (Baroghel-Bouny et al., 1999) for hardened cement pastes) and 0.99. Therefore, for the experimental data of (Maruyama et al., 2018), two calculations scenarios will be tested (named *Sc1* and *Sc2*) for the calculation of the drying shrinkage strains: for scenario *Sc1*, we consider that $S_w(h_R = 0.97) = 0.85$ and for scenario *Sc2* we consider that $S_w(h_R = 0.97) = 0.99$. The BJH results for both scenarios are shown in the following section. For each of those scenarios, we can calculate a volume V_{m0} (per unit of dry mass) and respectively a dry density[6]. The calculated values for the dry densities are respectively 1120 kg/m^3 and 1320 kg/m^3 for scenarios *Sc1* and *Sc2*. Those dry densities will be used posteriorly to calculate the specific surface area A_0 per unit volume (Table 3).

4.5.2 Results of the BJH analysis applied to experimental data

In this section, we show the obtained BJH results in terms of the saturated volume fraction of pores S_L compared to the experimental water degree saturation S_w and in terms of the surface fraction of the unsaturated pores ω_G.

For the experimental data of (Maruyama et al., 2018), the results are shown in Fig. 8-a and Fig. 8-b. In terms of saturation, for a relative humidity approximately equal to 0.35, the fraction of the saturated pores decreases sharply: the material loses a significant amount of the free liquid water. When the relative humidity h_R becomes smaller than *0.3*, a small part of the pores remains saturated (S_L ≈10%) until reaching approximately h_R=*0.03*. Below this relative humidity, all the water that remains in the pores is adsorbed water. In Fig. 8-b is shown the surface fraction ω_G of the unsaturated pores as a function of the relative humidity h_R. The specific surface area used to compute ω_G is the one obtained with the BET method (Table 1). For these curves, the same trends are observed as for S_L. It should be noted that in the purpose of judging the consistency of the BJH results, (Rouquerol, 2003) indicates that one must check that the specific surface area S_{BJH} calculated with the BJH method does not differ more than 10% from the specific surface area S_{BET} calculated with the BET method. This verification has been done with a calculated BJH surface area of 154 m^2/g compared to 157 m^2/g to that obtained with the BET method, which results in a difference of 2%. As for the two tested calculation scenarios *Sc1* and *Sc2*, we can note that in terms of saturation (Fig. 8-a) the two scenarios differ principally in the high range of relative humidity (i.e., for h_R >0.3). In terms of the calculated surface fraction of the unsaturated pores (Fig. 8-b), the difference is negligible.

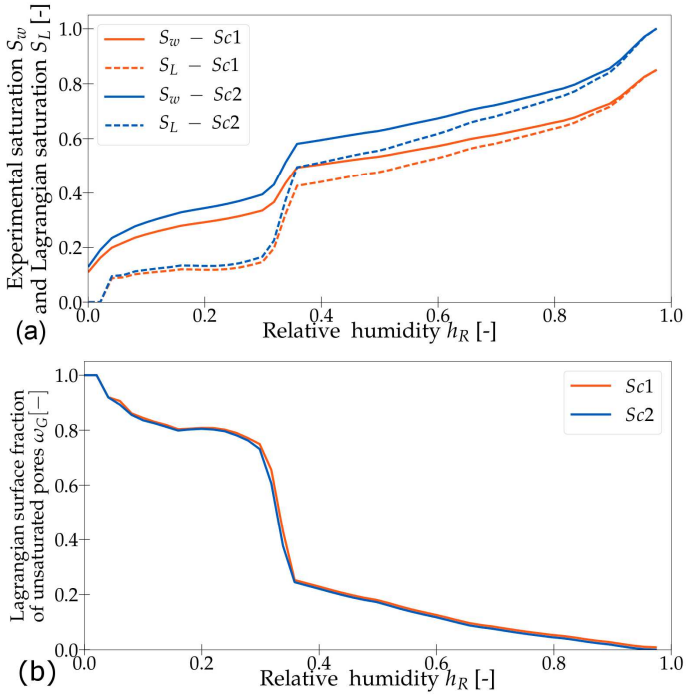

Fig. 8 – (a) and (b): variations of Lagrangian liquid saturation S_L, water degree saturation S_w and Lagrangian surface fraction ω_G of unsaturated pores, respectively, for the experimental data of (Maruyama et al., 2018)

The obtained BJH results for the experimental data of (Baroghel-Bouny et al., 1999) are presented in Fig. 9: when the relative humidity reaches a value of 0.55, S_L decreases sharply (Fig. 9-a) and the material loses a significant amount of liquid water from the saturated fraction of the pores. Below a relative humidity of 0.33, a small fraction of pores remains saturated

[6] $S_w = V_w/(\phi_0 V_{m0})$ where the volume of water in the pores V_w (per unit of dry mass) is calculated from the experimental water content (per unit of dry mass) given by (Maruyama et al., 2018) ($V_w = w/\rho_w$). For a given value of S_w ($h_R = 0.97$), w ($h_R = 0.97$) and ϕ_0=21%, we can calculate a volume V_{m0} (per unit of dry mass). The dry mass will be equal to $\rho_{dry} = 1/V_{m0}$

($S_L \approx 10\%$) until reaching a value of h_R=0.11 at which all pores become unsaturated. For the calculation of ω_G (shown in Fig. 9-b), the specific surface area used is the one calculated with the BET method (Table 1). The specific surface area calculated with the BJH is equal to 26.5 m²/g, which results in a difference of 2% with respect to the 27 m²/g calculated with the BET method.

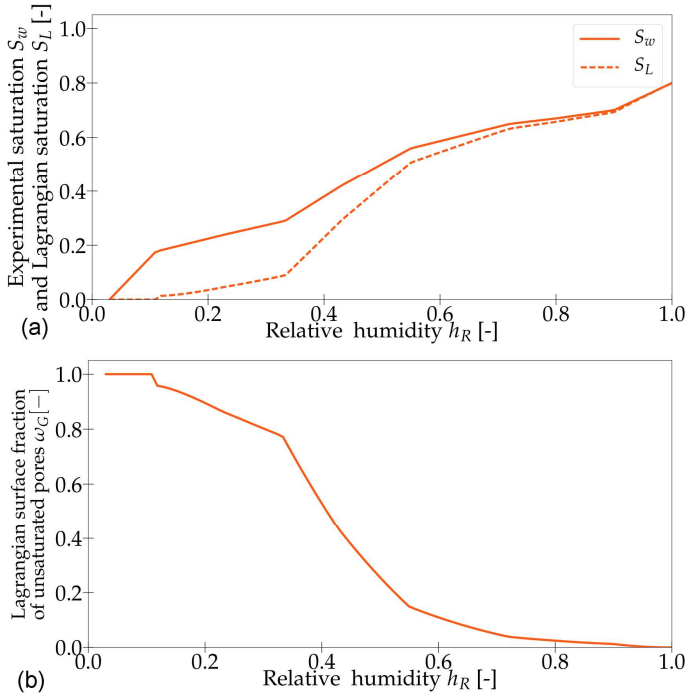

Fig. 9- (a) and (b): – (a) and (b): variations of Lagrangian liquid saturation S_L, water degree saturation S_w and Lagrangian surface fraction ω_G of unsaturated pores, respectively, for the experimental data of (Baroghel-Bouny et al., 1999)

Finally, for the experimental data of (Amberg and McIntosh, 1952) given in Fig. 10, when the relative humidity h_R reaches a value of 0.59 all the pores becomes unsaturated. Below this value, water will be found only under an adsorbed form. The main difference between the results obtained for the Vycor glass and for the previously tested cement materials is that Vycor glass tends to remain saturated during the initial stages and then to release sharply all the liquid water in a very narrow range of relative humidity h_R (in this example in a range between 0.7 and 0.59). (Vlahinić et al., 2009) linked this behavior to the morphology of the Vycor glass: contrary to cementitious materials, this material shows a narrow pore size distribution, with a majority of pores in the nanometer range (Scherer, 1986). On another hand, the specific surface area S_{BJH} calculated with the BJH method is 100 m²/g. A difference of 20% with the specific surface area S_{BET} = 81 m²/g (see Table 1) calculated with the BET method is noted. As previously explained, this difference could be due to an underestimation of S_{BET} linked to the limited number of experimental points used for the BET computation. Consequently, having an order of magnitude similar to specific surface areas of Vycor glasses found in the literature (see section 4.3), the specific surface area of 100 m²/g calculated with the BJH method will be retained for processing the (Amberg and McIntosh, 1952) experimental data. The corresponding calculated values of the Lagrangian surface fraction ω_G ($=\sum_i \delta a_{p,i} / S_{BJH}$) of unsaturated pores is shown in Fig. 10-b and is compared to the calculated values of ω_G ($=\sum_i \delta a_{p,i} / S_{BET}$).

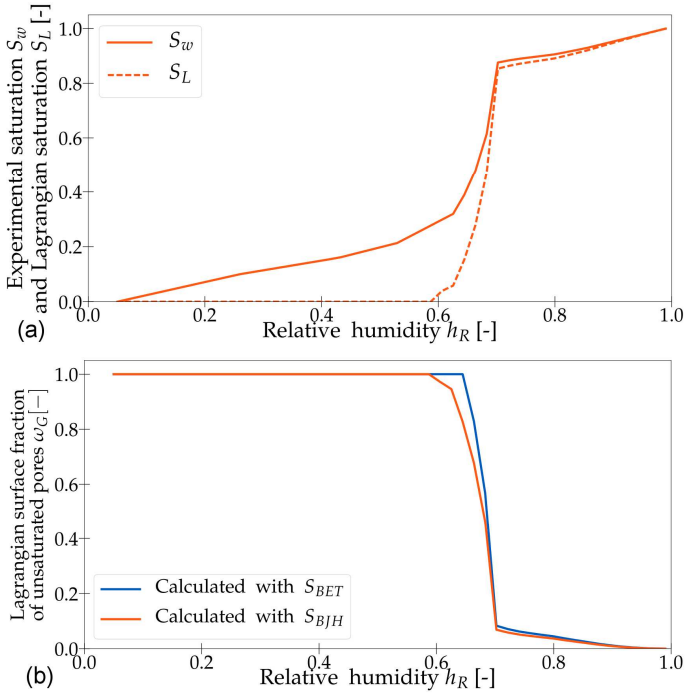

Fig. 10- (a) and (b): variations of Lagrangian liquid saturation S_L, water degree saturation S_w and Lagrangian surface fraction ω_G of unsaturated pores, respectively, for the experimental data of (Amberg and McIntosh, 1952)

Another important input parameter of the model is the specific surface area per unit volume A_0 (m^2/m^3): this value is calculated from the product of the previously calculated specific surface area (m^2/g) with the dry density (kg/m^3) for each of the tested materials. The calculated values are shown in Table 3.

Experimental Data	***Specific surface area*** **(m^2/g)**	***Dry density*** **(kg/m^3)**	A_0 **(m^2/m^3)**
(Maruyama et al., 2018) – *Sc1*	157	1120	$1.76\ 10^{+08}$
(Maruyama et al., 2018) – *Sc2*	157	1320	$2.07\ 10^{+08}$
(Baroghel-Bouny et al., 1999)	27	2382	$6.43\ 10^{+07}$
(Amberg and McIntosh, 1952)	100	1450	$1.45\ 10^{+08}$

Table 3- Calculated specific surface areas per unit volume

The previously computed quantities $S_L(h_R)$, $\omega_G(h_R)$ and A_0 will be used as input parameters for the calculation of the equivalent pore pressure (equation (47)) and of the drying shrinkage strains (equation (48)). The corresponding results are shown in the following section.

It should be noted that in (Maruyama et al., 2018), for the cement paste studied in this work (and other studied cementitious porous bodies) the sudden drop observed in the experimental water content for a relative humidity h_R near 0.35 was explained by the cavitation phenomena, that causes no liquid water to be found in the pores for a relative humidity h_R below approximately 0.35: "During adsorption or desorption, the surface tension acting on the meniscus causes negative pressure in the condensed liquid water […].When the negative pressure in the liquid water becomes too large, the liquid water becomes unstable, the nucleation of vapor bubbles must occur and suddenly a certain amount of water is released from the sample." Nonetheless, even though the previously presented BJH results (Fig. 8 and Fig. 9) showed a sharp decrease in the liquid water amount S_L for a relative humidity near 0.35, no total desaturation of the pores (i.e. $S_L \neq 0$) was observed for this value of relative humidity. Therefore, aiming at studying the impact of considering such an allegation, an alternative BJH computation method is shown in the appendix. This method consists on using the BJH technique until reaching a h_R near 0.35 and then to assume complete desaturation of the pores ($S_L = 0$ and $\omega_G = 1$). The impact of this method on the calculation of the drying shrinkage strains is presented in the appendix.

On another hand, as described earlier (§ 4.5.1), the BJH calculation could give an approximate value for the average radii of pores found in a studied porous material. Given that the poromechanical approach developed in this work is only valid for porous materials presenting macro and meso pores, the BJH calculation could therefore indicate approximately when micropores (if present) start to get emptied and hence under which relative humidity the developed model could lose its validity. According to the BJH results, micropores (with an average pore size < 2 nm) could be found for relative humidities smaller than approximately 20% for the studied hcp and high performance concrete and smaller than 25% for the Vycor glass. Therefore, it is important to note that while the stresses and strains are calculated (in the following section) for ranges of relative

humidities down to 3%, the calculated values for relative humidities smaller than 20%-25% could be considered only as approximate values.

4.6 Results and discussion

4.6.1 Equivalent pore pressure and drying shrinkage strains

In order to compute the drying shrinkage strains, by referring to equation (48), two important parameters are needed: the Biot coefficient b and the elastic bulk modulus K_b of the porous medium. Due to the uncertainties in the value of the Biot coefficient, this parameter is not fixed but chosen to vary within a range, whereas the value of K_b is fixed. Results in terms of drying shrinkage strains are then given and discussed based on the defined range, by testing both the upper and the lower bound of b.

In the article of (Maruyama et al., 2018), no values were provided for the two parameters K_b and b. Therefore, to be consistent with the previously assumed porosity of the studied hcp, we refer again to the work of (Di Bella et al., 2017), which provide for K_b the value of 14.8 GPa. As for the elastic bulk modulus K_s of the solid skeleton, (Di Bella et al., 2017) refer to the works of (Grasley et al., 2007) and (Hashin and Shtrikman, 1963) and indicate a range of variation for this parameter: $38\ \text{GPa} \leq K_s \leq 55\ \text{GPa}$. Making use of the classical relation $b = 1 - K_b/K_s$, the given range of variation of K_s together with the adopted value of K_b leads to a range of variation of the Biot coefficient b: $0.61 \leq b \leq 0.73$.

In the same way, in the article of (Baroghel-Bouny et al., 1999), the values of K_b and b for the studied concrete were not provided. We refer then to the work of (Brue et al., 2017) where for a similar high-performance concrete the authors note: $K_b = 30.8$ GPa and $b = 0.55$. We consider a range of variation of the Biot coefficient for the high-performance concrete between 0.55 and 0.7.

Finally concerning the studied Vycor glass, in the works of (Vlahinić et al., 2009), a value of $K_b = 7.2$ GPa is given based on the works of (Scherer, 1986). K_s is indicated in the range $19\ \text{GPa} \leq K_s \leq 23.6\ \text{GPa}$ based on the works of (Amberg and McIntosh, 1952). This range of K_s, for the given value of K_b, leads to a range of variation of Biot coefficient b between 0.62 and 0.7.

In what follows, results are given for each set of experimental data first in terms of drying shrinkage strains (Fig. 11-a, Fig. 12, Fig. 13-a and Fig. 14-a) and then of the equivalent pore pressure (see Fig. 11-b, Fig. 13-b and Fig. 14-b). As for the equivalent pore pressure, the contribution of each term is also shown, with the following notation:

- Contribution of the average pore pressure effect ($P_G - S_L P_C$) also written as ($S_G P_G + S_L P_L$) in dark blue.
- Contribution of the interfaces energy effect ($\frac{2}{3}\int_{S_{100}}^{S_L} P_c(S_L)\, dS_L$) in orange.
- Contribution of the fluid adsorption effect ($\frac{2}{3}(A_0/\phi_0)(\int_0^{\mu} \omega_G\, \Gamma\, d\mu$)) in light blue.
- Contribution of the Shuttleworth effect ($\frac{2}{3}(A_0/\phi_0)(-\left(\frac{\partial \gamma}{\partial \varepsilon_s}\right)\Big|_{\mu} \omega_G)$)) in yellow.
- Equivalent pore pressure π in green.

Together with the equivalent pore pressure and individual contributions, the Lagrangian saturation S_L (dashed magenta curve) and the Lagrangian surface fraction of unsaturated pores ω_G (dashed blue curve) are also presented to associate them to the various contributions.

First, we discuss the results obtained with the experimental data of (Maruyama et al., 2018) while taking scenario *Sc1* into account (Fig. 11). The calculated drying shrinkage strains compared to the experimental ones are given in Fig. 11-a. In solid lines, we represent the obtained model results for both tested values of Biot coefficient b while neglecting the Shuttleworth effect (i.e. by setting the term $\left(\frac{\partial \gamma}{\partial \varepsilon_s}\right)\Big|_{\mu}$ in expression (47) equal to zero). In dashed lines, we represent the results obtained for both tested values of Biot coefficient b while fitting the Shuttleworth term on the drying shrinkage experimental points. The obtained values for this term are $3.96\ 10^{-8}$ (MN/m) when b=0.61 and $7.29\ 10^{-10}$ (MN/m) when b=0.73. It is important to note that when b=0.73, the term $\frac{\partial \gamma}{\partial \varepsilon_s}$ is of a small order of magnitude compared to that of surface energies found in the literature (for instance, for a water-air interface at ambient temperature, γ_{GL} =73.10^{-03} (N/m) (Coussy, 2010)). By referring to the Shuttleworth equation given by (10), the previous observation leads to presume that the value of the surface stress σ_s at the solid/gas interface is very close to that of the interfaces surface energy γ and thus that the Shuttleworth effect at this interface is negligible. As for the obtained results, when b is taken equal to 0.61, fitting the Shuttleworth term allows to better model the drying shrinkage strains. In contrast, when b is taken equal to 0.73, fitting this parameter has no impact on the modeling results, which are already quite satisfactory. Due to the lack of information necessary to identify an exact value for the Shuttleworth term, both tested solutions shown in Fig. 11-a (considering zero fit parameter or fitting the Shuttleworth term) can be retained.

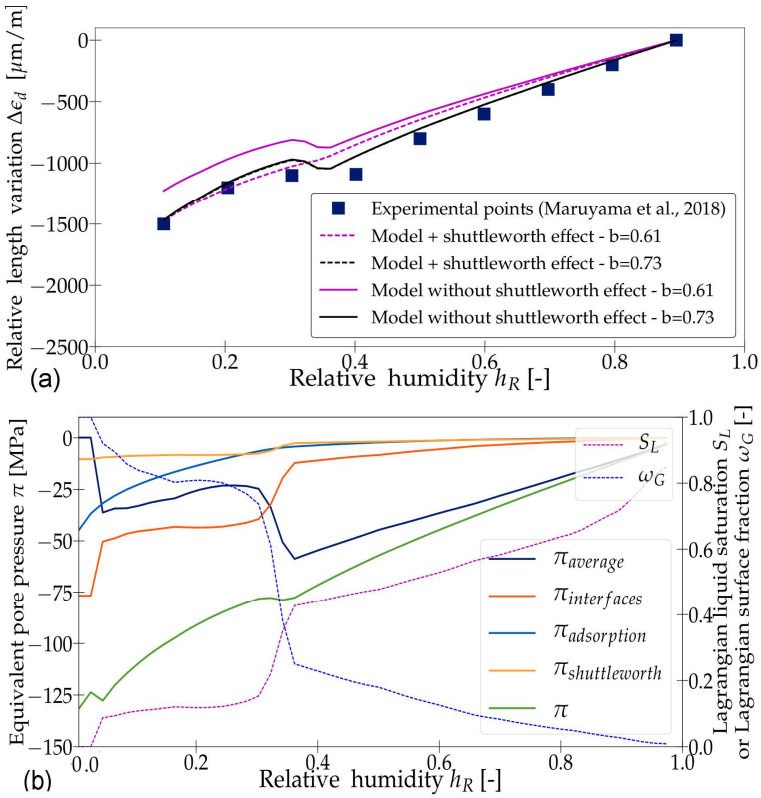

Fig. 11 – Results for the experimental data of (Maruyama et al., 2018) with the calculation scenario *Sc1*: (a) Calculated relative length variations with $\frac{\partial\gamma}{\partial\varepsilon_s}$ = 3.96 10^{-8} (MN/m) when b=0.61 and 7.29 10^{-10} (MN/m) when b=0.73
(b) Contributions to the equivalent pore pressure

The equivalent pore pressure π with the different contributions are displayed in Fig. 11-b. The Shuttleworth contribution shown in this figure corresponds to a fit of the Shuttleworth term while taking an average value for the Biot coefficient (b=0.67). At first sight, it could be noticed that in the high relative humidity range (h_R*>0.35),* the average pore pressure contributes most importantly in the development of the equivalent pore pressure, whereas in the low relative humidity range (h_R*<0.35)* interfaces energy and adsorption effects contribute primarily.

We can also observe that the average pore pressure and the interfaces energy contributions seem somehow correlated to the liquid saturation S_L. In fact, when during desorption, the material loses sharply a significant amount of capillary water (S_L drops sharply near h_R=*0.35*), the contribution of the interfaces energy increases in a similar way and the contribution of the average pore pressure decreases accordingly. In the range 0.03<h_R*<0.3,* the amount of liquid water in the pores becomes very small and varies very slightly, and similarly the interfaces energy effect and the average pore pressure effect in this range of relative humidity vary, but only slightly. When the relative humidity reaches 0.03, the material loses all the remaining liquid water and the liquid saturation S_L becomes equal to 0. At this stage, the contribution of the average pore pressure drops to zero whereas the contribution of the interfaces energy increases sharply to reach a plateau.

In regards to the contribution of the adsorption effect, the latter is controlled by two important parameters: the parameter ω_G and the parameter Γ which is directly linked to the thickness t of the adsorbed layer of water. The fact that the thickness t decreases with a decreasing relative humidity h_R on the whole range of relative humidity leads to a continuous increase of the adsorption stresses σ_s with a decreasing relative humidity.

Concerning the Shuttleworth effect, the corresponding contribution to the equivalent pore pressure is found to be negligible when compared to those of the other effects, and that over the whole range of relative humidity.

Finally, it may be concluded that, for this studied case, the proposed model appears to give satisfactory results (especially when b is near 0.73) even when the Shuttleworth effect is neglected. A small improvement of the results can be provided when a Shuttleworth parameter is fitted on experimental results.

The same evaluation has been done for the calculation scenario *Sc2* of the experimental data of (Maruyama et al., 2018). The corresponding calculated drying shrinkage strains are shown in Fig. 12.

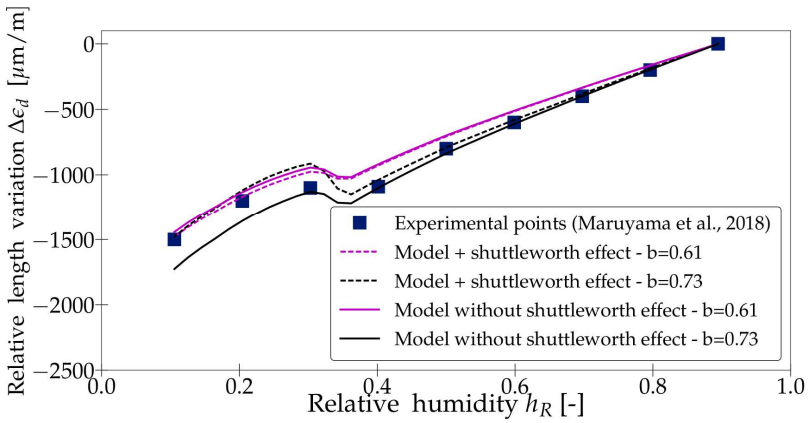

Fig. 12- Calculated relative length variation for the experimental data of (Maruyama et al., 2018) with the calculation scenario *Sc2* with $\frac{\partial\gamma}{\partial\varepsilon_s}$ = 4.95 10^{-9} (MN/m) when b=0.61 and -2.8 10^{-08} (MN/m) when b=0.73

Similar to the previous considered scenario, the same conclusion could be drawn. The results given by the proposed model while assuming a negligible Shuttleworth effect appear to be quite satisfactory. Taking into account a fit parameter can lead to a small improvement of the results. On another hand, it can be deduced that taking into account a calculation scenario *Sc1* (with an experimental degree of saturation $S_w\,(h_R = 0.97) = 0.85)$ or a calculation scenario *Sc2* (with an experimental degree of saturation $S_w(h_R = 0.97) = 0.99$) for the studied experimental data of (Maruyama et al., 2018) shows a small impact on the modeling results.

On another hand, the analysis done with the experimental data of (Baroghel-Bouny et al., 1999) leads to the results shown in Fig. 13.

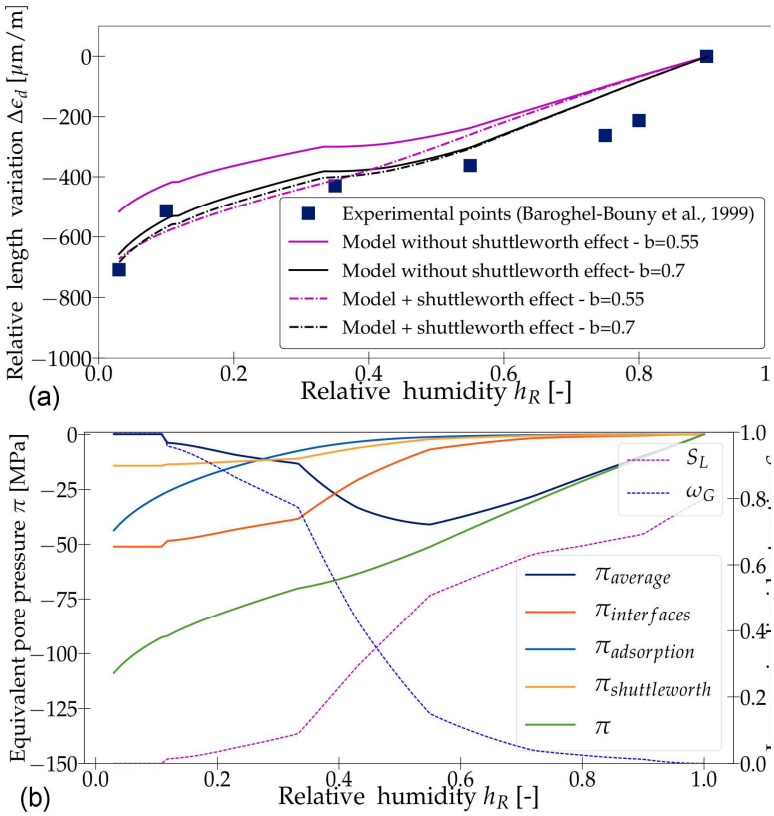

Fig. 13 – Results for the experimental data of (Baroghel-Bouny et al., 1999): (a) Calculated relative length variation with $\left(\frac{\partial\gamma}{\partial\varepsilon_s}\right)\Big|_{\mu}$ = 4.97 10^{-8} (MN/m) for b=0.55 and 6.88 10^{-9} (MN/m) for b=0.7- (b) Contributions to the equivalent pore pressure

Regarding the contributions to the equivalent pore pressure (see Fig. 13-b), the same comments done previously with the experimental data of (Maruyama et al., 2018*)* apply, while noting an important contribution of the average pore pressure for relative humidities larger than approximately 0.5 in this case. When the remaining amount of liquid water in the pores becomes small, the adsorption effects and the interfaces energy effect are the primordial contributions to the increase of the equivalent pore pressure. Regarding the Shuttleworth effect (that corresponds to a fit of the Shuttleworth term for an average value of $b = 0.62$*)*, equally in this case, its contribution to the equivalent pore pressure is considered to be small with respect to other effects contributions. The previously drawn conclusions can be made: the model gives satisfactory results when neglecting the Shuttleworth effect (especially when we take a Biot coefficient of 0.7). Taking into account a parameter to fit the Shuttleworth effect can slightly refine the modeling results.

Finally, the results obtained with the experimental data of (Amberg and McIntosh, 1952) are shown in Fig. 14. Fig. 14-b indicates a major role of the average pore pressure when the relative humidity is larger than 0.7 (i.e. when the majority of the pores are filled with liquid water) whereas below this value the effect of the interfaces energy and the fluid adsorption effects take the lead. The Shuttleworth effect contribution (for an average value of $b = 0.66$) could also be considered negligible with respect to other effects contributions on the total range of h_R. As for the drying shrinkage strains in Fig. 14-a, identically in this case, we can conclude that, when neglecting the Shuttleworth effect, the model provided satisfactory results for the studied range of Biot coefficients b (especially when b is taken equal to 0.7).

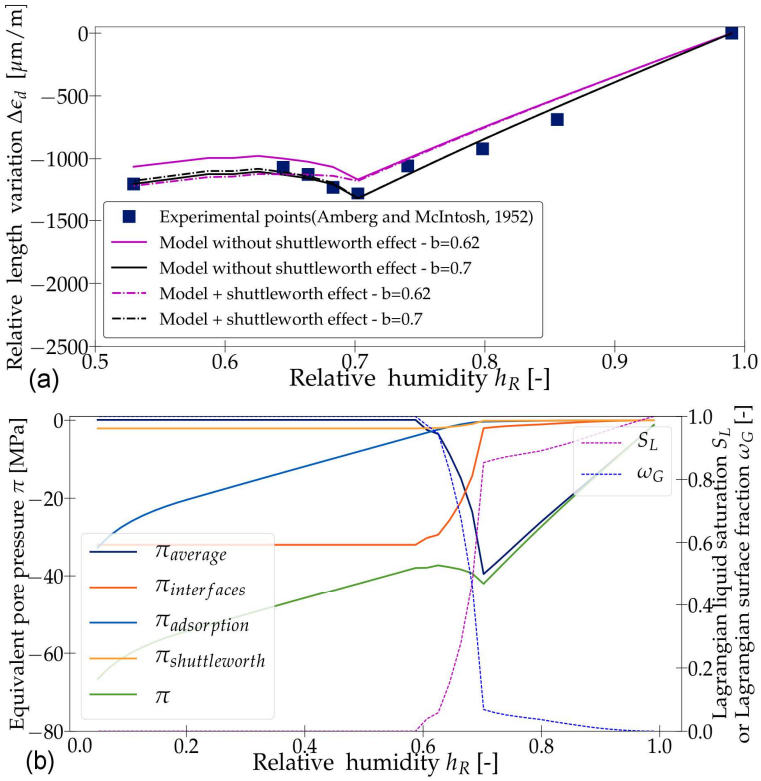

Fig. 14 – Results for the experimental data of (Amberg and McIntosh, 1952): (a) Calculated relative length variation with $\left(\frac{\partial\gamma}{\partial\varepsilon_s}\right)\Big|_\mu$ = 1.51 10^{-8} (MN/m) for b=0.62 and -2.19 10^{-9} (MN/m) for b=0.7- (b) Contributions to the equivalent pore pressure

Last but not least, beyond the estimation of correct values for the Biot coefficient and the Shuttleworth parameter, it is shown in all previous results that the proposed model is able to correctly evaluate drying shrinkage strains on the whole range of relative humidity. Moreover, the proposed model is capable of capturing the remarkable plateau in drying shrinkage strains observed at intermediate relative humidity. This plateau represents a transition in the relative contribution to the increase of the equivalent pore pressure, from the average pore pressure effects (in the high h_R range) to the interfaces energy and the adsorption effects (in the low h_R range).

On another hand, we believe that the stresses and pressures (of 100 MPa) created at the scale of the microstructure of the porous materials should not be interpreted as macro stresses which could eventually cause some micro cracks when then tension threshold of cementitious materials is exceeded. We believe that those micro stresses could be submitted to some kind of microstructural relaxation before acting on the macro scale.

4.6.2 Comparison of the proposed model with the Biot-Bishop and the (Coussy et al., 2003) models

In this section, we aim to compare the newly proposed poromechanical with a classical Biot-Bishop model (equation (2)) and the (Coussy et al., 2003) model (equation (3)) in their ability to predict drying shrinkage strains.Comparisons are done while considering negligible Shuttleworth effect, i.e. by considering $\left(\frac{\partial \gamma}{\partial \varepsilon_s}\right)\Big|_{\mu} = 0$. Both the upper and lower bounds of the Biot coefficient were tested for each set of experimental data. The results (see Fig. 15) show a good estimation of the drying shrinkage strains by the three models in the higher range of relative humidity.

In this range, the average pore pressure is the main contributor to the equivalent pore pressure. This range corresponds more precisely to relative humidities larger than approximately 0.4 for the cementitious material studied in (Maruyama et al., 2018) and (Baroghel-Bouny et al., 1999) and than approximately 0.7 for those of (Amberg and McIntosh, 1952).

Nevertheless, in the low range of relative humidity, the Biot-Bishop model shows less satisfactory results. In fact, this model is strongly impacted by the experimental method adopted to measure the experimental degree of saturation S_w. More specifically, it is affected by the choice of the dry reference state (Di Bella et al., 2017). Indeed, as it can be seen in Fig. 15-c and Fig. 15-d, this model can even predict a swelling of the material instead of a shrinkage. On another hand, regarding the (Coussy et al., 2003) model, it is observed that the latter can lead to an over-estimation of the drying shrinkage strains in the low range of relative humidity. Moreover, it should be pointed out that this model predicts an approximately constant slope over the whole range of h_R. The latter observation has been previously made in the works of (Di Bella et al., 2017) and (Wyrzykowski et al., 2017). In contrast to the previous models, the proposed model provides a better estimation of the drying shrinkage strains especially when the Biot coefficient is near 0.7. In addition, this model permits to clearly capture the transition (pointed out with the dashed frames of Fig. 15) at which contributions to the effective pore pressure stem mostly from the average pore pressure on one hand, and mostly from the fluid adsorption and interfaces energy effects on the other hand.

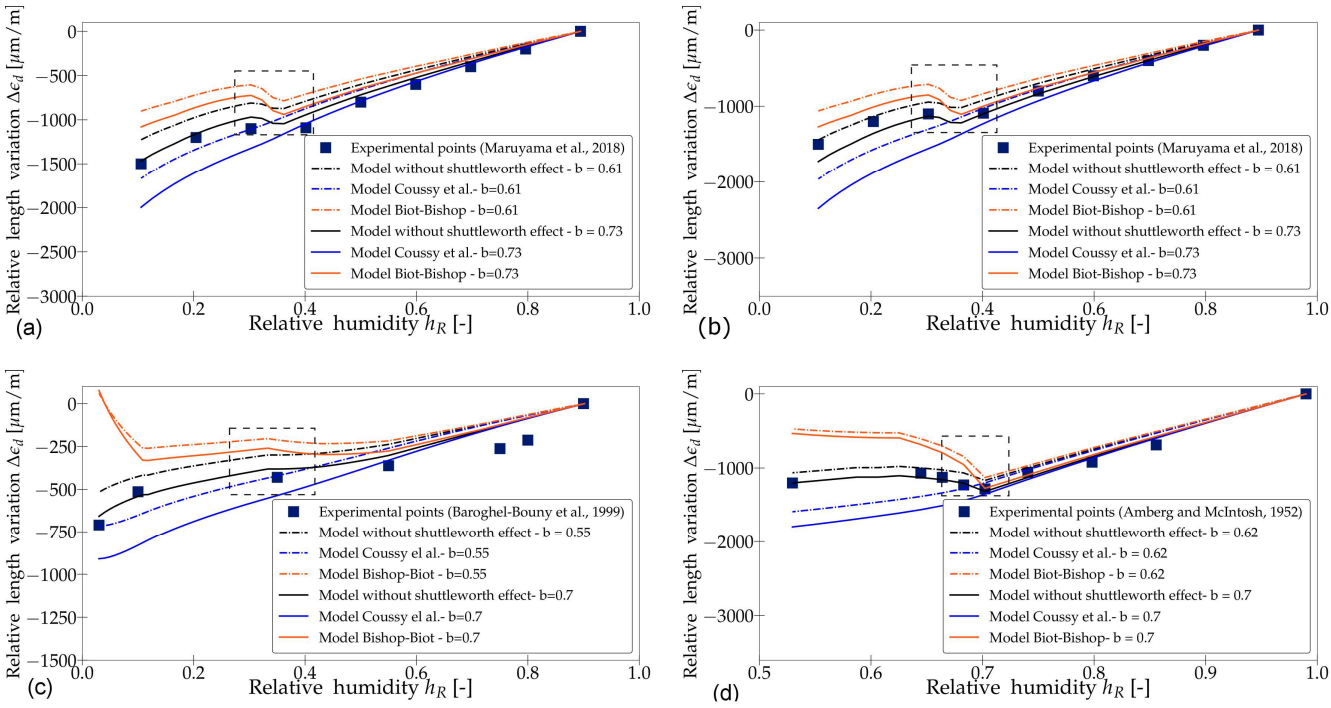

Fig. 15- Comparison of the current model with the Biot-Bishop and the (Coussy et al.,2003) models for the experimental data of: (a) (Maruyama et al., 2018) with the calculation scenario *Sc1*– (b) (Maruyama et al., 2018) with the calculation scenario *Sc2*– (c) (Baroghel-Bouny et al., 2018)- (d) (Amberg and McIntosh, 1952)

5 Conclusions

In this work, the macroscopic poromechanical approach for unsaturated bodies has been revisited and extended to the low relative humidity ranges to model the drying processes. By adopting a proper thermodynamical derivation, we derived a new model that allows to account for different contributions in the development of the effective stresses such as the average pore pressure effects, the interfaces energy effects, the fluid adsorption effects and the Shuttleworth effect.

Regarding the input parameters, this model requires essentially the use of two commonly known techniques for the identification of features of the pores structures: the BET theory (Brunauer et al., 1938) and the BJH technique (Barrett et al.,

1951). Even though the BJH technique does not always qualify as the best technique to characterize pores size, in the current framework this technique was used because of its coherence with the developed poromechanical approach.

The poromechanical model has been tested and validated on experimental results (water desorption curves and drying shrinkage strains curves) found in the literature. Different porous materials are studied, such as an ordinary cement paste from the works of (Maruyama et al., 2018), a high-performance concrete tested by (Baroghel-Bouny et al., 1999) and a Vycor glass tested by (Amberg and McIntosh, 1952).

By applying the newly developed model to the mentioned experimental data, we have shown that the average pore pressure is the main contributor to the strains/stresses development in the higher relative humidity range (i.e., for relative humidities larger than approximately 0.4 for cementitious materials and than 0.7 for Vycor Glass). In the low relative humidity range, both interfaces energy effects and fluid adsorption effects play an important role. Regarding the Shuttleworth effect (which captures the variation of the surface energy with respect to the skeleton strains), due to the fact that the magnitude of the effect cannot be assessed in an evident way a priori, we proposed to fit the parameter that governs its magnitude (i.e. the term $\left(\frac{\partial \gamma}{\partial \varepsilon_s}\right)\Big|_{\mu}$) on experimental data drying shrinkage strains. From previous results, we came to realize that the contribution of the Shuttleworth effect to the development of the equivalent pore pressure is negligible when compared to the contribution of the other effects.

As for the estimated drying shrinkage strains, for the experimental data on which we validated our model, exact values of the Biot coefficient were not provided. Hence, we considered a range for this parameter, based on literature works. Both the upper and the lower bounds of this range have been tested, for all studied materials. For the materials considered, even when neglecting the Shuttleworth term, our model can give a good estimation of the drying shrinkage strains when the coefficient of Biot is equal to 0.7. It should be noted that this approach does not take into account the long-term viscous deformations. However, those deformations could be accounted for by the adjustment of the Biot coefficient while checking that the value of the latter remains within reasonable limits.

Finally, the drying shrinkage strains estimated with the proposed model when neglecting the Shuttleworth effect have been compared to those obtained with a classical Biot-Bishop model and the model of (Coussy et al., 2003). All three poromechanical models gave good results in the higher range of relative humidity. However, in contrast to those two models, we showed that the proposed model is not only capable of successfully evaluating drying shrinkage strains for low relative humidity but more specifically to predict a noticeable plateau in the evolution of the drying shrinkage strains, which also appears in the considered experimental data sets. In our model, this plateau represents the transition between a contribution to the effective pore pressure stemming mostly from the average pore pressure (at high relative humidity) on one hand, and stemming mostly from interfaces energy and adsorption of fluid (at low relative humidity) on the other hand.

Appendix 1

In this appendix, we show the results obtained when we consider that for a certain value of relative humidity h_R near 0.35, cavitation will take place (as stated in (Maruyama et al., 2018)). Below this value of relative humidity, all pores will be considered unsaturated. In terms of the model parameters, this corresponds to fixing $S_L(h_R) = 0$ and $\omega_G(h_R) = 1$ for a relative humidity smaller than approximately 0.35.

Concerning the experimental data of (Maruyama et al., 2018), the complete desaturation of pores is considered for a relative humidity h_R=*0.3*. This value has been chosen based on previous observations (refer to Fig. 8 : when the relative humidity reaches a value near 0.3, the hcp is left with a value of S_L near zero). As done previously, for the experimental data of (Maruyama et al., 2018), the two scenarios *Sc1* (Fig A1.*1*) and *Sc2* (Fig A1.*2*) were equally tested. The obtained curves $S_L(h_R)$ and $\omega_G(h_R)$from the BJH computation are presented respectively in Fig A1.*1*-b and Fig A1.*2*-b. The calculated drying shrinkage strains are shown Fig A1.-a for the calculation scenario *Sc1* and Fig A1.1-a for the calculation scenario *Sc2*. The equivalent pore pressure and the corresponding contributions are shown in Fig A1.1-b and Fig A1.2-b respectively for scenarios *Sc1* and *Sc2*.

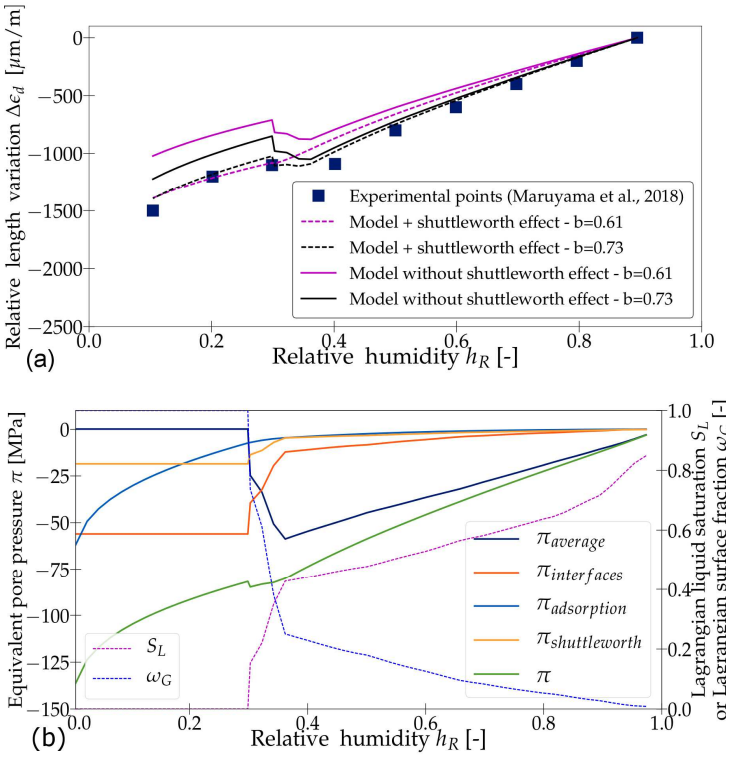

Fig A1.1–Results for the experimental data of (Maruyama et al., 2018) with the calculation scenario *Sc1*: (a) Calculated relative length variations– (b) Contributions to the equivalent pore pressure

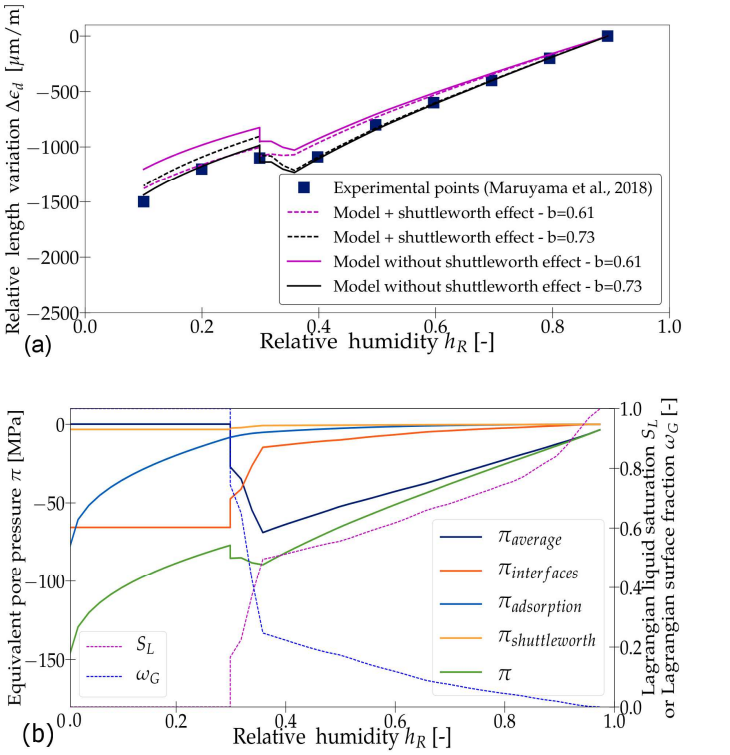

Fig A1.2– Results for the experimental data of (Maruyama et al., 2018) with the calculation scenario *Sc2*: (a) Calculated relative length variations– (b) Contributions to the equivalent pore pressure

Regarding the experimental results of (Baroghel-Bouny et al., 1999), the BJH calculation was stopped at a relative humidity h_R of 0.33. Below this value, pores are assumed to be totally unsaturated. This value has been chosen based on previous observations (see Fig. 9: when the relative humidity reaches 0.33, the studied concrete is left with a very small amount of liquid water). The BJH curves $S_L(h_R)$ and $\omega_G(h_R)$ and model results are shown in Fig A.3. From the previous results, we can conclude that if the BJH computation was stopped at a value of relative humidity h_R near 0.35 and total desaturation of pores was assumed for this value, this may lead (as seen in Fig A1.*1*-a) to a less satisfactory prediction of the drying shrinkage strains when neglecting the Shuttleworth effect and considering a value of b near 0.7. Therefore, the BJH method detailed in section 4.5 (where the BJH computation is maintained until approaching 0% of relative humidity) should be retained for further model predictions.

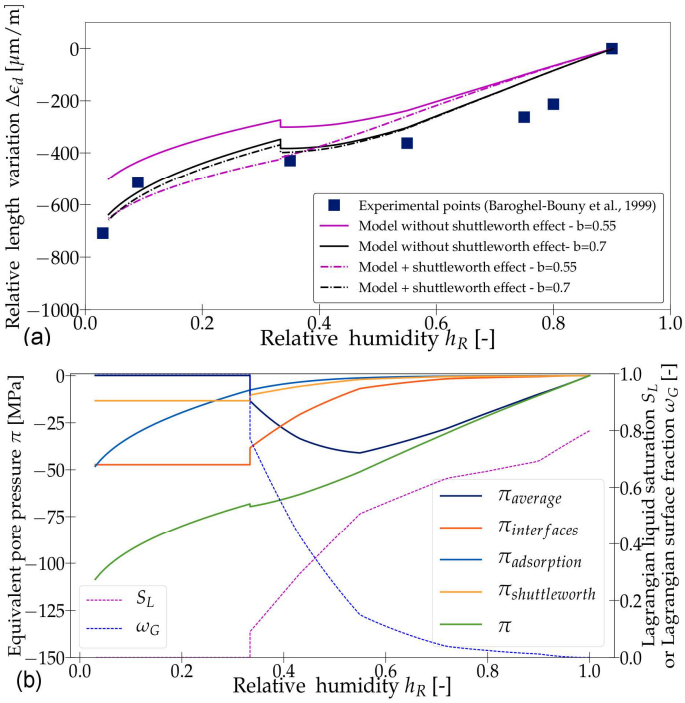

Fig A.3– Results for the data of (Baroghel-Bouny et al., 1999): (a) Calculated relative length variations – (b) Contributions to the equivalent pore pressure

Appendix 2

In this appendix, we verify the previous indication that states that any isotropic homothetic variation of the pore dimension by a factor $(1+\lambda/3)$ will induce a volume increase of $(1+\lambda)$ and a surface increase of $(1+\frac{2\lambda}{3})$ regardless of the considered shape of the pore. For this purpose, let us consider first a spherical shaped pore with a radius r and lets us note the factor $\lambda/3$ as β :

- The initial volume of the pore is $V_i = \frac{4}{3}\pi r^3$ and its initial surface is $S_i = 4\pi r^2$

- If we consider an isotropic homothetic variation of the pores by a factor $(1+\beta)$ then the final volume of the sphere will be equal to $V_f = \frac{4}{3}\pi(r(1+\beta))^3 = \frac{4}{3}\pi r^3(1+\beta)^3$. If we consider only the first order terms, we could write $V_f = \frac{4}{3}\pi r^3(1+3\beta)$ and thus the increase of the volume of the sphere is of $(1+3\beta)$.

- The final surface is $S_i = 4\pi\big(r(1+\beta)\big)^2 = 4\pi r^2(1+\beta)^2$. If we consider only the first order terms, we could write $S_f = 4\pi r^2(1+2\beta)$ and thus the increase of the surface of the sphere is of $(1+2\beta)$.

The same demonstration could be done for pore with a shape of an infinite cylinder with a radius r and a height h:

- The initial volume of the pore is $V_i = \pi r^2 h$ and its initial surface is $S_i = 2\pi rh$

- If we consider an isotropic homothetic variation of the pores by a factor $(1+\beta)$ then the final volume of the cylinder will be equal to $V_f = \pi(r(1+\beta))^2(h(1+\beta)) = \pi r^2 h(1+\beta)^3$. If we consider only the first order terms, we could write $V_f = \pi r^2 h(1+3\beta)$ and thus the increase of the volume of the sphere is of $(1+3\beta)$.

- The final surface is $S_i = 2\pi(r(1+\beta))(h(1+\beta)) = 2\pi rh(1+\beta)^2$. If we consider only the first order terms, we could write $S_f = 2\pi rh(1+2\beta)$ and thus the increase of the surface of the sphere is of $(1+2\beta)$.

References

Aligizaki, K.K., 2006. Pore structure of cement-based materials : testing, interpretation and requirements. Taylor & Francis.

Amberg, C.., McIntosh, R., 1952. A Study of Adsorption Hysteresisby Means of length changes of a rod of porous glass. Can. J. Chem. 30, 1012–1032.

Andrieu, S., Muller, P., 2005. Les surfaces solides: concepts et méthodes.

Badmann, R., Stockhausen, N., Setzer, M.J., 1981. The statistical thickness and the chemical potential of adsorbed water films. J. Colloid Interface Sci. 82, 534–542. https://doi.org/10.1016/0021-9797(81)90395-7

Balzer, C., Waag, A.M., Gehret, S., Reichenauer, G., Putz, F., Hüsing, N., Paris, O., Bernstein, N., Gor, G.Y., Neimark, A. V., 2017. Adsorption-Induced Deformation of Hierarchically Structured Mesoporous Silica - Effect of Pore-Level Anisotropy. Langmuir 33, 5592–5602. https://doi.org/10.1021/acs.langmuir.7b00468

Bangham, D.H., 1931. The Swelling of Charcoal. Proc. R. Soc. London, Ser. A 130, 81–89.

Bangham, D.H., Fakhoury, N., Mohamed, a. F., 1934. The Swelling of Charcoal. Part III. Experiments with the Lower Alcohols. Proc. R. Soc. A Math. Phys. Eng. Sci. 147, 152–175. https://doi.org/10.1098/rspa.1934.0212

Baroghel-Bouny, 1994. Caractérisation microstructurale et hydrique des pâtes de ciment et des bétons ordinaires e at es hautes performances.

Baroghel-Bouny, V., 2007. Water vapour sorption experiments on hardened cementitious materials. Part II: Essential tool for assessment of transport properties and for durability prediction. Cem. Concr. Res. 37, 438–454. https://doi.org/10.1016/j.cemconres.2006.11.017

Baroghel-Bouny, V., Mainguy, M., Lassabatere, T., Coussy, O., 1999. Characterization and identification of equilibrium and transfer moisture properties for ordinary and high-performance cementitious materials. Cem. Concr. Res.

Barrett, Joyner, Halenda, 1951. BJH analysis 1896. https://doi.org/10.1021/ja01145a126

Beltzung, F., Wittmann, F.H., 2005. Role of disjoining pressure in cement based materials. Cem. Concr. Res. 35, 2364–2370. https://doi.org/10.1016/j.cemconres.2005.04.004

Bentz, D.P., Garboczi, E.J., Quenard, D.A., 1998. Modelling drying shrinkage in reconstructed porous materials: Application to porous Vycor glass. Model. Simul. Mater. Sci. Eng. 6, 211–236. https://doi.org/10.1088/0965-0393/6/3/002

Biot, M.A., 1941. General theory of three-dimensional consolidation. J. Appl. Phys. 12, 155–164. https://doi.org/10.1063/1.1712886

Biot, M.A., Willis, D.G., 1957. The elastic coefficients of the theory of consolidation. J. appl. Mech 594–601. https://doi.org/10.1002/9780470172766.ch13

Bishop, A.W., Blight, G.E., 1963. Some Aspects of Effective Stress in Saturated and Partly Saturated Soils. Géotechnique 13, 177–197. https://doi.org/10.1680/geot.1963.13.3.177

Brue, F.N.G., Davy, C.A., Burlion, N., Skoczylas, F., Bourbon, X., 2017. Five year drying of high performance concretes: Effect of temperature and cement-type on shrinkage. Cem. Concr. Res. 99, 70–85. https://doi.org/10.1016/j.cemconres.2017.04.017

Brunauer, S., Emmett, P.H., Teller, E., 1938. Adsorption of Gases in Multimolecular Layers. J. Am. Chem. Soc. 60, 309–319. https://doi.org/10.1021/ja01269a023

Cammarata, R.C., 1994. Surface and interface stress effects in thin films. Prog. Surf. Sci. 46, 1–38. https://doi.org/10.1016/0079-6816(94)90005-1

Chen, W., 2013. Etude expérimentale de la perméabilité du béton sous conditions thermiques et hydriques variables.

Coussy, O., 2010. Mechanics and Physics of Porous Solids, Mechanics and Physics of Porous Solids. https://doi.org/10.1002/9780470710388

Coussy, O., 2007. Revisiting the constitutive equations of unsaturated O Coussy To cite this version : HAL Id : hal-00359952 Revisiting the constitutive equations of unsaturated porous solids using a Lagrangian saturation concept. https://doi.org/10.1002/nag.613

Coussy, O., 2004. Poromechanics, John Wiley & Sons. https://doi.org/10.1002/0470092718

Coussy, O., Dangla, P., Lassabatere, T., Baroghel-Bouny, V., 2003. The equivalent pore pressure and the swelling and shrinkage of cement-based materials. Mater. Struct. 37, 15–20. https://doi.org/10.1617/14080

Dangla, P., Pereira, J., 2014. A Thermodynamic Approach to Effective Stresses in Unsaturated Soils Incorporating the Concept of Partial Pore Deformations. https://doi.org/10.2136/vzj2013.06.0110

Di Bella, C., Wyrzykowski, M., Lura, P., 2017. Evaluation of the ultimate drying shrinkage of cement-based mortars with poroelastic models. Mater. Struct. Constr. 50, 1–13. https://doi.org/10.1617/s11527-016-0870-0

Durner, W., 1994. Hydraulic Conductivity Estimation for Soils with Heterogeneus pore Structure. Water Resour. Res.

Gawin, D., Pesavento, F., Schrefler, B.A., 2006. Hygro-thermo-chemo-mechanical modelling of concrete at early ages and beyond. Part II: Shrinkage and creep of concrete. Int. J. Numer. Methods Eng. 67, 332–363. https://doi.org/10.1002/nme.1636

Gibbs, J.W.A. du texte, 1928. The collected works / of J. W. Gibbs,...

Gor, G.Y., Bernstein, N., 2016a. Revisiting Bangham's law of adsorption-induced deformation: changes of surface energy and surface stress. Phys. Chem. Chem. Phys. 18, 9788–9798. https://doi.org/10.1039/C6CP00051G

Gor, G.Y., Bernstein, N., 2016b. Revisiting Bangham's law of adsorption-induced deformation: Changes of surface energy and surface stress. Phys. Chem. Chem. Phys. 18, 9788–9798. https://doi.org/10.1039/c6cp00051g

Gor, G.Y., Huber, P., Weissmüller, J., 2018. Elastocapillarity in nanopores : Sorption strain from the actions of surface tension and surface stress 086002, 1–17. https://doi.org/10.1103/PhysRevMaterials.2.086002

Grasley, Z.C., Scherer, G.W., Lange, D.A., Valenza, J.J., 2007. Dynamic pressurization method for measuring permeability and modulus: II. cementitious materials. Mater. Struct. Constr. 40, 711–721. https://doi.org/10.1617/s11527-006-9184-y

Gyozo G., L., Cesar A., B., 2012. Laser Techniques for the Study of Electrode Processes. Springer, Dordrecht, The Netherlands.

Hagymassy, J., Brunauer, S., Mikhail, R.S., 1969. Pore structure analysis by water vapor adsorption. J. Colloid Interface Sci. Volume 29, p485-491.

Hashin, Z., Shtrikman, S., 1963. A variational approach to the theory of the elastic behaviour of multiphase materials. J. Mech. Phys. Solids 11, 127–140. https://doi.org/10.1016/0022-5096(63)90060-7

Hassanizadeh, S.., Gray, W.., 1980. General conservation equations for multi-phase systems: 3. Constitutive theory for porous media flow. Adv. Water Ressources 3, 25–40.

Hiller, K.H., 1964. Strength Reduction and Length Changes in Porous Glass Caused by Water Vapor Adsorption. J. Appl. Phys. 35, 1622–1628. https://doi.org/10.1063/1.1713697

Hutter, K., Laloui, L., Vulliet, L., 1999. Thermodynamically based mixture models of saturated and unsaturated soils. Mech. Cohesive-frictional Mater. 4, 295–338. https://doi.org/10.1002/(SICI)1099-1484(199907)4:4<295::AID-CFM64>3.0.CO;2-9

IAPWS, 1992. The International Association for the Properties of Water and Steam: Revised Supplementary Release on Saturation Properties of Ordinary Water Substance 10, 1–7.

Koenders, E.A.B., Van Breugel, K., 1997. Numerical modelling of autogenous shrinkage of hardening cement paste. Cem. Concr. Res. 27, 1489–1499. https://doi.org/10.1016/S0008-8846(97)00170-1

Kovler, K., Zhutovsky, S., 2006. Overview and future trends of shrinkage research. Mater. Struct. Constr. 39, 827–847. https://doi.org/10.1617/s11527-006-9114-z

Kramer, D., Weissmüller, J., 2007. A note on surface stress and surface tension and their interrelation via Shuttleworth's equation and the Lippmann equation. Surf. Sci. 601, 3042–3051. https://doi.org/10.1016/J.SUSC.2007.05.005

Lewis, R.W. (Roland W., Schrefler, B.A., 1987. The finite element method in the deformation and consolidation of porous media. Wiley.

Lura, P., Jensen, O.M., Van Breugel, K., 2003. Autogenous shrinkage in high-performance cement paste: An evaluation of basic mechanisms. Cem. Concr.

Res. 33, 223–232. https://doi.org/10.1016/S0008-8846(02)00890-6
Maruyama, I., 2010. Origin of Drying Shrinkage of Hardened Cement Paste: Hydration Pressure. J. Adv. Concr. Technol. 8, 187–200. https://doi.org/10.3151/jact.8.187
Maruyama, I., Rymeš, J., Vandamme, M., Coasne, B., 2018. Cavitation of water in hardened cement paste under short-term desorption measurements. Mater. Struct. Constr. 51. https://doi.org/10.1617/s11527-018-1285-x
Maugis, D., 1980. Cahiers du Groupe Français de RhéolQgie 5.
Mjahad, S., 2012. Impact de la fissuration sur les propriétés de rentention d'eau et de transport de gaz.Application au stockage profond des déchets radioactifs.
Morandeau, A., Sellier, A., Denis, R., Rapporteur, D., Examinateur, B.H., Scrivener, K., 2014. Carbonatation atmosphérique des systèmes cimentaires à faible teneur en portlandite.
Nguyen, H., Rahimi-Aghdam, S., Bažant, Z.P., 2020. Unsaturated nanoporomechanics. Proc. Natl. Acad. Sci. 201919337. https://doi.org/10.1073/pnas.1919337117
Nguyen, H.T., Rahimi-Aghdam, S., Bažant, Z.P., 2019. Sorption isotherm restricted by multilayer hindered adsorption and its relation to nanopore size distribution. J. Mech. Phys. Solids 127, 111–124. https://doi.org/10.1016/j.jmps.2019.03.003
NIST Chemistry WebBook, 2018. NIST Chemistry WebBook,Thermophysical Properties of Fluid Systems [WWW Document]. SRD69.
Pereira, J.-M., Coussy, O., Alonso, E.E., Vaunat, J., Olivella, S., 2010. Is the degree of saturation a good candidate for Bishop's X parameter? Alonso, E.E., Gens, A. Unsaturated Soils—Proceedings 5th Int. Conf. Unsaturated Soils 913–919. https://doi.org/1010.2608
Powers, T.C., Brownyard, T.L., 1947. Studies of the Physical Properties of Hardened Portland Cement Paste. Res. Lab. Portl. Cem. Assoc. https://doi.org/10.14359/15301
Rahimi-Aghdam, S., Masoero, E., Rasoolinejad, M., Bažant, Z.P., 2019. Century-long expansion of hydrating cement counteracting concrete shrinkage due to humidity drop from selfdesiccation or external drying. Mater. Struct. Constr. 52. https://doi.org/10.1617/s11527-018-1307-8
Rahoui, H., 2018. Contribution à la compréhension de l'action des agents réducteurs de retrait dans les matériaux cimentaires: étude expérimentale et modélisation. http://www.theses.fr.
Ravikovitch, P.I., Neimark, A. V., 2006. Density functional theory model of adsorption deformation. Langmuir 22, 10864–10868. https://doi.org/10.1021/la061092u
Rougelot, T., Skoczylas, F., Burlion, N., 2009. Water desorption and shrinkage in mortars and cement pastes: Experimental study and poromechanical model. Cem. Concr. Res. 39, 36–44. https://doi.org/10.1016/j.cemconres.2008.10.005
Rouquerol, F. et al., 2003. Texture des matériaux pulvérulents ou poreux. Tech. l'Ingénieur P1050, 1–24.
Scherer, G., 1986. Dilatation of Porous Glass. J. Am. Ceram. Soc. 69, 473–480. https://doi.org/10.1111/j.1151-2916.1986.tb07448.x
Schulman, R.D., Trejo, M., Salez, T., Raphaël, E., Dalnoki-Veress, K., 2018. Surface energy of strained amorphous solids. Nat. Commun. 9, 8–13. https://doi.org/10.1038/s41467-018-03346-1
Setzer, M., Duckheim, C., 2009. Drying shrinkage mechanisms of hardened cement paste, in: Creep, Shrinkage and Durability Mechanics of Concrete and Concrete Structures. pp. 49–55. https://doi.org/10.1201/9780203882955.ch6
Setzer, M.J., Duckheim, C., Liebrecht, A., Kruschwitz, J., 2006. the Solid-Liquid Gel-System of Hardened Cement Paste 1–16.
Shuttleworth, R., 1950. The Surface Tension of Solids. Proc. Phys. Soc. Sect. A 63, 444–457. https://doi.org/10.1088/0370-1298/63/5/302
Thomas, J.J., Jennings, H.M., Allen, A.J., 1999. The surface area of hardened cement paste as measured by various techniques. Concr. Sci. Eng. https://doi.org/10.1016/S0008-8846(98)00049-0
Van-Genuchten, 1980. A closed-form equation for predicting the hydraulic conductivity of unsaturated soils.
Vandamme, M., Brochard, L., Lecampion, B., Coussy, O., 2010. Adsorption and strain: The CO2-induced swelling of coal. J. Mech. Phys. Solids 58, 1489–1505. https://doi.org/10.1016/j.jmps.2010.07.014
Vlahinić, I., Jennings, H.M., Thomas, J.J., 2009. A constitutive model for drying of a partially saturated porous material. Mech. Mater. 41, 319–328. https://doi.org/10.1016/j.mechmat.2008.10.011
Weber, B., Ehrhardt, J.-J., Thomy, A., 1988. Surface des solides. Tech. l'ingénieur 33, 0–20.
Wittmann, F.H., 2008. Heresies on shrinkage and creep mechanisms. Proc. 8th Int. Conf. Creep, Shrinkage Durab. Mech. Concr. Concr. Struct. (CONCREEP 8) 8, 3–9. https://doi.org/10.1201/9780203882955.pt1
Wyrzykowski, M., Bella, C.D., Lura, P., 2017. Prediction of Drying Shrinkage of Cement-Based Mortars with Poroelastic Approaches - A Critical Review. Poromechanics 2017 - Proc. 6th Biot Conf. Poromechanics 579–586. https://doi.org/10.1061/9780784480779.071
Zhang, Y., 2018. Mechanics of adsorption–deformation coupling in porous media. J. Mech. Phys. Solids 114, 31–54. https://doi.org/10.1016/j.jmps.2018.02.009